Cellular/Molecular

Synaptic Integration of Subquantal Neurotransmission by Colocalized G Protein-Coupled Receptors in Presynaptic Terminals

Emily Church,[1,3*] Edaeni Hamid,[2,3*] Zack Zurawski,[1] Mariana Potcoava,[1] Eden Flores-Barrera,[1] Adriana Caballero,[1] Kuei Y. Tseng,[1] and Simon Alford[1]

[1]Department of Anatomy and Cell Biology, University of Illinois at Chicago, Chicago, Illinois 60612, [2]Department of Biological Sciences, University of Illinois at Chicago, Chicago, Illinois 60607, and [3]Graduate Program in Neuroscience, University of Illinois at Chicago, Chicago, Illinois 60612

In presynaptic terminals, membrane-delimited $G_{i/o}$-mediated presynaptic inhibition is ubiquitous and acts via G$\beta\gamma$ to inhibit Ca^{2+} entry, or directly at SNARE complexes to inhibit Ca^{2+}-dependent synaptotagmin-SNARE complex interactions. At CA1-subicular presynaptic terminals, 5-HT_{1B} and $GABA_B$ receptors colocalize. $GABA_B$ receptors inhibit Ca^{2+} entry, whereas 5-HT_{1B} receptors target SNARE complexes. We demonstrate in male and female rats that $GABA_B$ receptors alter P_r, whereas 5-HT_{1B} receptors reduce evoked cleft glutamate concentrations, allowing differential inhibition of AMPAR and NMDAR EPSCs. This reduction in cleft glutamate concentration was confirmed by imaging glutamate release using a genetic sensor (iGluSnFR). Simulations of glutamate release and postsynaptic glutamate receptor currents were made. We tested effects of changes in vesicle numbers undergoing fusion at single synapses, relative placement of fusing vesicles and postsynaptic receptors, and the rate of release of glutamate from a fusion pore. Experimental effects of P_r changes, consistent with $GABA_B$ receptor effects, were straightforwardly represented by changes in numbers of synapses. The effects of 5-HT_{1B} receptor-mediated inhibition are well fit by simulated modulation of the release rate of glutamate into the cleft. Colocalization of different actions of GPCRs provides synaptic integration within presynaptic terminals. Train-dependent presynaptic Ca^{2+} accumulation forces frequency-dependent recovery of neurotransmission during 5-HT_{1B} receptor activation. This is consistent with competition between Ca^{2+}-synaptotagmin and G$\beta\gamma$ at SNARE complexes. Thus, stimulus trains in 5-HT_{1B} receptor agonist unveil dynamic synaptic modulation and a sophisticated hippocampal output filter that itself is modulated by colocalized $GABA_B$ receptors, which alter presynaptic Ca^{2+}. In combination, these pathways allow complex presynaptic integration.

Key words: fusion pore; membrane delimited; presynaptic calcium; presynaptic G proteins; synaptic integration; synaptic vesicle fusion

Significance Statement

Two G protein-coupled receptors colocalize at presynaptic sites, to mediate presynaptic modulation by G$\beta\gamma$, but one (a $GABA_B$ receptor) inhibits Ca^{2+} entry whereas another (a 5-HT_{1B} receptor) competes with Ca^{2+}-synaptotagmin binding to the synaptic vesicle machinery. We have investigated downstream effects of signaling and integrative properties of these receptors. Their effects are profoundly different. $GABA_B$ receptors alter P_r leaving synaptic properties unchanged, whereas 5-HT_{1B} receptors fundamentally change properties of synaptic transmission, modifying AMPAR but sparing NMDAR responses. Coactivation of these receptors allows synaptic integration because of convergence of $GABA_B$ receptor alteration on Ca^{2+} and the effect of this altered Ca^{2+} signal on 5-HT_{1B} receptor signaling. This presynaptic convergence provides a novel form of synaptic integration.

Received Jan. 6, 2021; revised Dec. 9, 2021; accepted Dec. 13, 2021.

Author contributions: E.C., E.H., Z.Z., M.P., A.C., K.Y.T., and S.A. designed research; E.C., E.H., Z.Z., M.P., E.F.-B., A.C., and S.A. performed research; E.C., E.H., Z.Z., and S.A. analyzed data; E.C., K.Y.T., and S.A. edited the paper; E.C., A.C., and S.A. wrote the paper; S.A. wrote the first draft of the paper.

This work was supported by National Institutes of Health Grants R01 MH084874 and R01 NS052699 to S.A., Grant R01 MH086507 to K.Y.T., and Grant F31 NS063662 to E.H. We thank Drs. Heidi Hamm, Janet Richmond, and Jonathan Art for helpful discussions throughout the course of this study and of this manuscript.

*E.C. and E.H. contributed equally to this work.

The authors declare no competing financial interests.

Correspondence should be addressed to Simon Alford at sta@uic.edu.

https://doi.org/10.1523/JNEUROSCI.0035-21.2021

Introduction

G protein-coupled receptors (GPCRs) control neurotransmitter release at all synapses via membrane delimited actions of G$\beta\gamma$ (Betke et al., 2012). Much attention has been placed on $G_{i/o}$ G protein modulation of Ca^{2+} entry (Tedford and Zamponi, 2006). This alters synaptic vesicle fusion probability (P_r) (Hessler et al., 1993), a phenomenon taken as proof of presynaptic action (Dobrunz and Stevens, 1997). However, at least one other membrane delimited action of G$\beta\gamma$ occurs. At synapses in lamprey, in amygdala, hippocampus, and in chromaffin and PC12 cells,

GPCRs modulate exocytosis via G$\beta\gamma$-(SNARE) complex interactions (Blackmer et al., 2001; Takahashi et al., 2001; Blackmer et al., 2005; X. K. Chen et al., 2005). This modulation is caused by G$\beta\gamma$ competition with synaptotagmin at c-terminal SNAP-25 on SNARE complexes of primed vesicles. Mutation of this SNAP-25/G$\beta\gamma$ interaction site in mice demonstrates central effects on anxiety, spatial memory, and motor control, as well as endocrine release and metabolism implying broad implications for this exocytotic modulation in brain and the periphery (Zurawski et al., 2019). The mechanistic effects of these different modulatory processes on synaptic transmission remain debated (Pawlu et al., 2004; Balaji and Ryan, 2007; Alabi and Tsien, 2013).

Because G$\beta\gamma$ directly interacts with SNARE complexes this opens new possibilities for the mechanistic effect of its signaling at presynaptic terminals. If G$\beta\gamma$ interacts with a subset of primed vesicles at the terminal, it might alter P_r at just those sites or it might change the mode of vesicle fusion (Elhamdani et al., 2006; Alabi and Tsien, 2013). If the synapse releases just one vesicle, if it is univesicular (Maschi and Klyachko, 2020), altering P_r changes the number of synaptic sites releasing transmitter for any given action potential. This will not alter transmitter concentration at each site. In contrast, variation in synaptic cleft neurotransmitter concentration might be caused by alterations in P_r within multivesicular release (MVR) synapses (Rudolph et al., 2015). Concentrations of transmitter at postsynaptic receptors might also be changed by altering the location of release sites within active zones with respect to the postsynaptic receptors (Tang et al., 2016). Finally, a change in synaptic cleft transmitter concentration may follow changes in vesicle fusion (Gandhi and Stevens, 2003). In the latter case, vesicle fusion begins with pore formation (Spruce et al., 1990), which expands to collapse the vesicle into the plasmalemma. The c-terminus of the SNARE complex protein SNAP-25 is required for this expansion (Fang et al., 2015). G$\beta\gamma$ interacts with SNARE complexes at this region of SNAP-25 to compete with Ca^{2+}-synaptotagmin interaction during evoked fusion (Zurawski et al., 2017). Thus, G$\beta\gamma$-SNARE interaction opens the possibility that GPCRs regulate the synaptic vesicle fusion mode and cleft neurotransmitter concentrations.

Because colocalized $GABA_B$ receptors modify Ca^{2+} entry and 5-HT_{1B} receptor effects are altered by Ca^{2+}, this provides a mechanism for presynaptic integration. We have previously demonstrated that colocalized but different $G_{i/o}$ GPCR-coupled receptors target G$\beta\gamma$ to different effectors. At CA1-subicular synapses, $GABA_B$ receptors reduce Ca^{2+} entry, and we now show, P_r, whereas 5-HT_{1B} receptors modify cleft glutamate concentrations of evoked vesicle fusion events to allow modulation of postsynaptic receptors. Neither of these mechanisms alters action potential invasion of the recorded synapses as demonstrated by reliability of action potential-evoked presynaptic Ca^{2+} transients (Hamid et al., 2014). With Monte Carlo simulation of glutamate release at modeled synapses, we reproduced experimental results supporting the hypothesis that $GABA_B$ receptors alter P_r at univesicular synapses, whereas 5-HT_{1B} receptor action is best explained by slowing glutamate release through a restricted fusion pore. This provides finer tuning of synaptic transmission than changes in P_r and creates a synaptic filter that selects for transmission of NMDAR-mediated events and trains of activity. We have now shown that $GABA_B$ receptors inhibit synaptic responses by changing P_r regardless of frequency. However, because they modify presynaptic Ca^{2+} entry which alters G$\beta\gamma$ competition with synaptotagmin at SNARE complexes, $GABA_B$ receptors cause meta-modulation by reshaping effects of 5-HT_{1B} receptors. Thus, presynaptic terminals show synaptic integration.

Materials and Methods

The preparation. Experiments were performed on hippocampal slices (300 μm) of 21- to 22-d-old male and female Sprague Dawley rats anesthetized with isoflurane and decapitated in accordance with institutional guidelines. Hippocampi were isolated under semi-frozen Krebs Henseleit solution (in mM as follows): 124 NaCl, 26 $NaHCO_3$, 1.25 NaH_2PO_4, 3 KCl, 2 $CaCl_2$, 1 $MgCl_2$, 10 D-glucose, bubbled with 95% O_2-5% CO_2, and sliced using a Vibratome (Leica VT1200, Leica Microsystems), except for experiments in which high Ca^{2+} concentrations were used. In these experiments to prevent calcium carbonate precipitation, bicarbonate buffer was substituted with HEPES using a solution of the following composition (in mM): 145 NaCl, 5 HEPES, 1.25 NaH_2PO_4, 3 KCl, 2 or 10 $CaCl_2$, 1 $MgCl_2$, 10 D-glucose, adjusted to pH 7.4 with NaOH and bubbled with O_2-100% CO_2. All recording were performed in a constant flow recording chamber in which the slices were held down with a harp. The recording chamber was superfused at ~2 ml/min and maintained at 28°C.

Electrophysiology. Subicular pyramidal neurons were whole-cell clamped by visual identification using an upright microscope illuminated via a fiber optic source. Recording used an Axopatch 200A or B amplifier (Molecular Devices). Patch pipettes (4-5 MΩ) contained solution (in mM as follows): cesium (for voltage clamp) or potassium methane sulfonate (for current clamp) 146, $MgCl_2$ 2, EGTA 5, HEPES 9.1, pH adjusted to 7.2 with CsOH or KOH. Series resistance was monitored by applying a 5-10 mV voltage step before each evoked synaptic response. If any series resistance change recorded during the experiment exceeded 20%, the cell was discarded from analysis. Focal stimuli (0.2 ms, ≤20 μA) were applied over CA1 axons using glass insulated monopolar tungsten microelectrodes (see Fig. 1*A*) (Hamid et al., 2014). Immediately after obtaining whole-cell access for up to 15 min, a hyperpolarization and reduction in impedance could sometimes be recorded on baclofen application. Baclofen activates postsynaptic G protein-activated inwardly rectifying K^+ currents to cause a change in postsynaptic impedance. This was not seen following CP93129 application. Nevertheless, in all recordings, including during those with baclofen, postsynaptic input impedance was tested with current pulses throughout the entirety of the experiment (see Fig. 4). However, the baclofen evoked reduction in impedance was lost after the initial 15 min period of recording. All experimental recordings of EPSCs were made after this initial period of recording, and no effect of baclofen on neuron impedance was recorded during any voltage-clamp experiments. Whole-cell impedance correction was not used during the experiment to avoid changes causing uncontrolled alterations in apparent EPSC amplitudes over the long recording period.

Expression of iGluSnFR in hippocampus. An AAV5 containing the glutamate sensor iGluSnFr under a human synapsin promoter was intracerebrally injected in rats at postnatal days 21-22. pAAV.hSyn.iGluSnFr.WPRE.SV40 was a gift from Loren Looger (Addgene, plasmid #98929). Briefly, rats were anesthetized with isoflurane during the stereotaxic surgery, and a volume of 0.2 μl of iGluSnFr was injected in the dorsal hippocampus at the following coordinates: AP: −4.0, ML: +/−2.7, and DV: −1.8. Hippocampal slices were prepared from these animals 7 and 14 d after the surgery using the same procedures as described for electrophysiological experiments.

Imaging experiments. Line-scan confocal imaging, as previously described (Hamid et al., 2019), was used for Ca^{2+} transient recording in presynaptic varicosities following single action potentials stimulated with somatic whole-cell electrodes. Alexa-594 hydrazide was excited at 568 nm. Fluo-5F was separately excited (488 nm) and imaged in bandpass (510-560 nm). Images were taken separately to ensure no cross-channel bleed-through. This was confirmed with neurons filled with only one dye. No bleed-through image was discernible for either dye to the incorrect channel. Varicosities were identified 20-35 min after whole-cell access by imaging the Alexa-594 hydrazide dye and tracking the axon from the filled soma to its

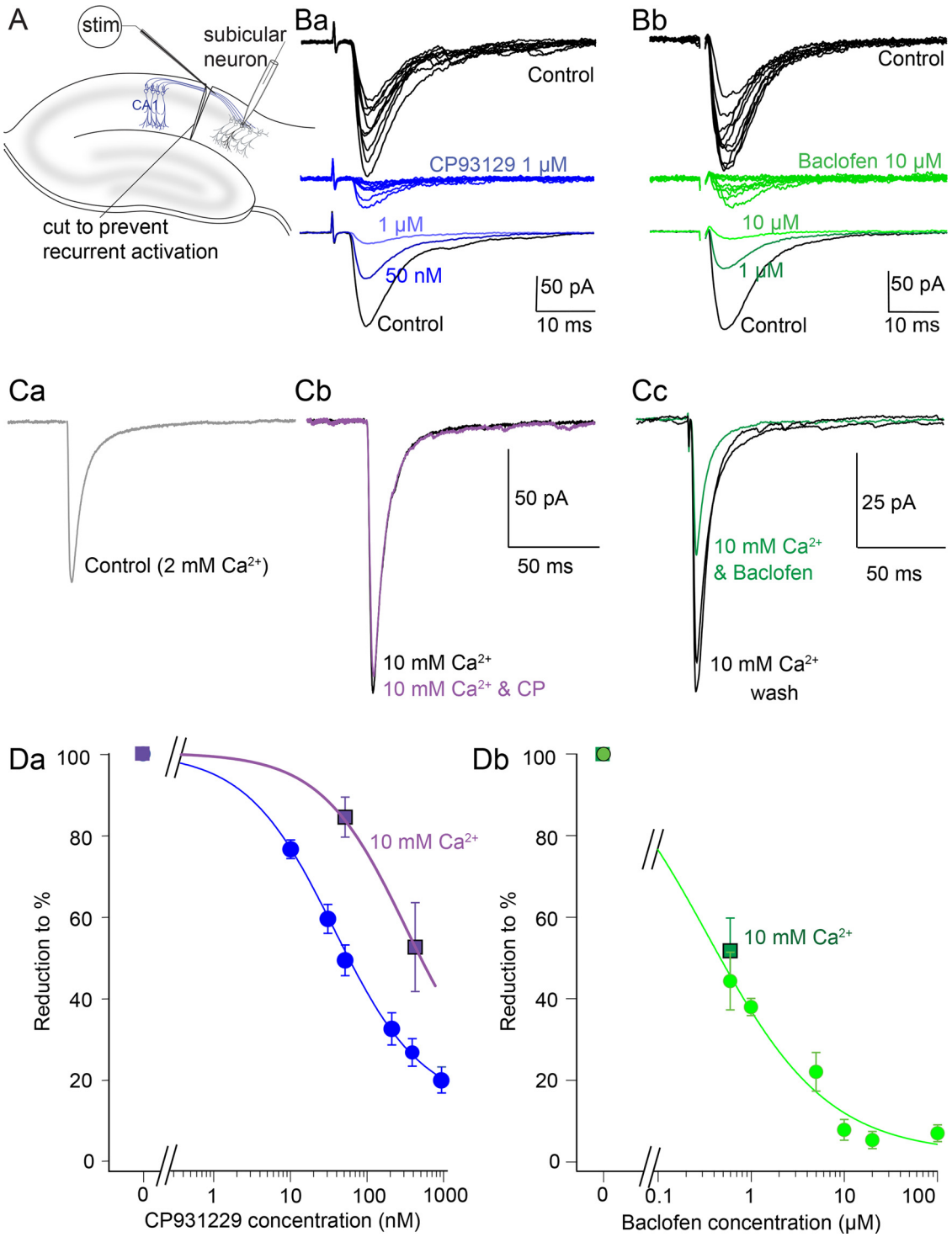

Figure 1. Presynaptic 5-HT_{1B} and $GABA_B$ receptors inhibit evoked transmission from CA1 pyramidal neurons. ***A***, Subicular pyramidal neurons were whole-cell patch-clamped. CA1 pyramidal axons were stimulated with a monopolar, glass-coated tungsten microelectrode. The tissue was cut at the CA1/subiculum boundary to prevent recurrent excitation. ***Ba***, Ten consecutive AMPAR-mediated EPSCs from a cell recorded in bicuculline (5 μM) and D-AP5 (50 μM) in control (black) and in CP93129 (blue). Means of responses in control (black) 50 nM (dark blue) and 1 μM CP93129 (blue) are shown below. ***Bb***, Similar evoked EPSCs were recorded in control (black) and baclofen (10 μM) green and means of EPSCs in control and in baclofen (1 μM, dark green) and 10 μM (green). ***C***, Synaptic responses recorded in control (***Ca***) after addition of 10 mM $CaCl_2$ (***Cb***, black) and with CP93129 (50 nM, purple). In raised extracellular Ca^{2+} (***Cc***), baclofen 1 μM inhibited the synaptic response as for controls. ***D***, Concentration responses for (***Da***) CP93129 in control saline (blue circles) and in 10 mM $CaCl_2$ (purple squares) and (***Db***) baclofen in control saline (light green circles) and in 10 mM $CaCl_2$ (dark green square).

projection into the subiculum. Ca^{2+} transients at these varicosities were imaged in line scanning mode (500 Hz) for up to 1 s during stimuli to the soma to evoke action potentials. Image analysis was performed within ImageJ, and images are represented as linear with the applied LUT mapping.

For Lattice Light Sheet Microscopy (LLSM) hippocampal slices were placed on cover slips previously coated with 50 mg/ml 300,000 MW poly-lysine in a perfused recording chamber under the LLSM objective lenses (see Fig. 6*A*). The LLSM was custom designed in our laboratory to allow simultaneous electrophysiology, but based on a Janelia Farm

Table 1. Monte Carlo simulation parameters and sources in Figures 7 and 8

Parameter	Value	Source
Glutamate diffusion constant ($cm^2 \cdot s^{-1}$)	3×10^{-6}	Rusakov and Kullmann, 1998
AMPAR parameters (glutamate)		
k1 ($M^{-1} \cdot s^{-1}$), k-1 (s^{-1})	2×10^7, 9×10^3	Robert and Howe, 2003
k-2 (s^{-1})	0.41	
γ_0, δ_0 (s^{-1})	1, 3×10^{-3}	
γ_1, δ_1 (s^{-1})	7.6, 1.8×10^3	
γ_2, δ_2 (s^{-1})	35, 200	
β, α (s^{-1})	8×10^3, 3.1×10^3	
Kynurenate		
k3 ($M^{-1} \cdot s^{-1}$)	5×10^7	Diamond and Jahr, 1997
k-3 (s^{-1})	9000	
NMDAR parameters		
on, off	95×10^5, 29	Banke and Traynelis, 2003
$d1^+$, $d1^-$	0.5, 45	
$d2^+$, $d2^-$	70, 2.8	
f^+, f^-	1557, 182	
s^+, s^-	89, 135	
Mesh properties		
Internal vesicle diameter (nm)	25	Hu et al., 2008
Pore length (nm)	8	Vardjan et al., 2007
Minimum pore diameter (nm)	0.4	Savtchenko and Rusakov, 2007
Synaptic cleft thickness (nm)	20	
Synaptic cleft diameter (nm)	300	Nimchinsky et al., 2002
Thickness of cleft edge diffusion barrier (nm)	1.7	Rusakov and Kullmann, 1998

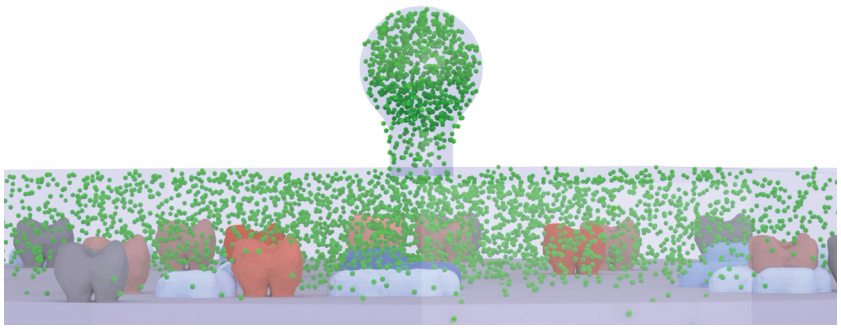

Movie 1. Simulation of vesicle pore opening an expansion. This movie shows the simulated synapse from the side demonstrating fusion of the vesicle compartment with the synaptic cleft, release of glutamate molecules (green), and binding of glutamate to postsynaptic AMPARs (red shades) and NMDARs (blue shades). Receptor colors depend on kinetic state (for kinetic models and colors, see Fig. 7*D*). [View online]

design (B. C. Chen et al., 2014). A twisted pair Nichrome stimulating electrode was positioned at the same location as electrophysiological experiments. Stimulation (200 µs, 5 s interval) evoked fluorescence transients stochastically across the 51 × 51 µm FOV. We imaged transients using LLSM at frame rates of up to 80 Hz in single planes across multiple hotspots in a single axon. Transients were imaged in sequential LLSM frames at the same *z* position.

Experimental design and statistical analyses. For all values of EPSC amplitude or fits to the EPSC rise and decays, the mean was taken of at least 10 evoked traces of EPSCs for each condition for each recorded neuron. Student's paired two-tailed *t* tests were used to calculate the significance of simple paired datasets. Comparison of multiple datasets under similar conditions was made using one-way ANOVA and, if necessary, followed with a *post hoc* Tukey HSD test for significance of each manipulation against all others. Results are presented as numbers of recordings (*n*), the values of the mean ± SEM, and for each statistical analysis are presented as degrees of freedom, *F* or *t* statistic, degrees of freedom, and absolute value of probability (*p*). *Post hoc* tests following significance obtained from an ANOVA give maximum values of *p* from tables. All values of *p* were from two-tailed tests. All replicates are from different neuronal recordings in different hippocampal slices.

Monte Carlo simulations. Monte Carlo simulations were applied to neurotransmitter release through an expanding model of a synaptic vesicle fusion pore within a simulated synapse. Simulations were run in the MCell environment (Kerr et al., 2008) in which a simple 3D mesh model of a synaptic cleft was created. The cleft was modeled as disk with a 300 nm diameter and a thickness of 20 nm. Neurotransmitter release was modeled from 1 to 3 vesicles with internal diameters of 25 nm fusing with expanding pores growing from 0.4 nm to complete opening to the diameter of the vesicle over a period varying from 200 µs to >20 ms. An example of the sequence of frames for a single pore and its expansion and loss of glutamate to the synaptic cleft is shown in Movie 1. Glutamate escape from the simulated synaptic cleft was slowed by limiting the thickness of the cleft at its edges. This was varied systematically to result in a glutamate decay to 10% of peak in 1 ms (Clements et al., 1992; Asztely et al., 1997) following the release of 5000 glutamate molecules. After escape from the cleft, glutamate molecules were removed from the model by simulating pumps external to the synaptic cleft. The vesicles were modeled containing from 700 to 20,000 glutamate molecules. Kinetic models of glutamate receptors were placed in the postsynaptic disk (20 NMDARs and 20 AMPARs) enabling simulation of the binding, activation, desensitization, inactivation, and unbinding of these receptors. Kinetic models of the receptors are shown in Figure 7. Model parameters, including those of the receptor kinetic models used, are included in Table 1. Animations of these simulations are shown in Movies 1 and 2.

Code accessibility. Simulation parameter files are available at https://alford.lab.uic.edu/GPCRs.html and at ModelDB for requested access (http://modeldb.yale.edu/266839) before publication of this work. This will be made public on publication. The authors declare that experimental data supporting the findings of this study are available within the paper.

Results

$GABA_B$ and 5-HT_{1B} receptors inhibit synaptic transmission from CA1 to subiculum

5-HT_{1B} and $GABA_B$ receptors have previously been shown to be coexpressed in CA1 axon presynaptic terminals (Boeijinga and Boddeke, 1996; Bonaventure et al., 1998; Lein et al., 2007; Hamid et al., 2014) where both receptors inhibit synaptic transmission, but by different mechanisms. We have previously shown that $GABA_B$ receptors inhibit Ca^{2+} entry, while 5-HT_{1B} receptors cause G$\beta\gamma$ to act directly at the SNARE complex (Hamid et al., 2014). The amount of inhibition of Ca^{2+} entry by $GABA_B$ receptors in that study was sufficient to account for the effect of the $GABA_B$ receptor agonist baclofen on synaptic transmission. In contrast, the effect of the 5-HT_{1B} receptor agonist CP93129 was eliminated by treatment of the tissue with botulinum A toxin to remove the c-terminal 9 residues from SNAP-25; and in a further study (Zurawski et al., 2019), genetic manipulation of the c-terminal of SNAP-25 also prevented 5-HT_{1B} receptor modulation of neurotransmitter release. We also showed in those studies no loss of transmission between soma and axons. This was indicated by Ca^{2+} transients that were unaffected by 5-HT_{1B} receptors and reduced in amplitude, but not prevented by $GABA_B$ receptors (Hamid et al., 2014).

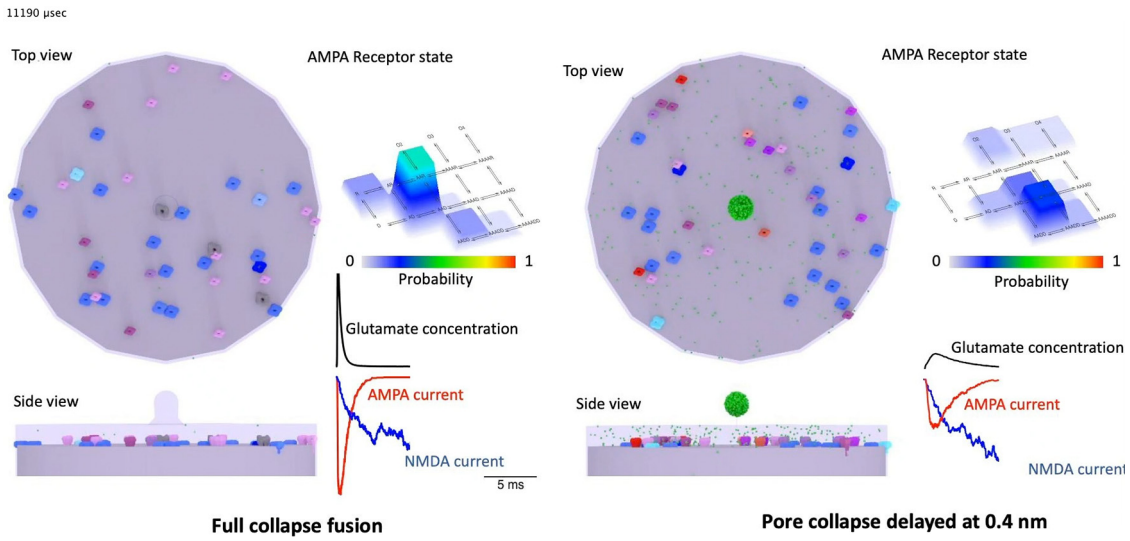

Movie 2. Simulations of full rapid fusion and delayed fusion pore opening. Left panels, Top and side views of vesicle fusing and releasing glutamate into the synaptic cleft. AMPAR state probabilities are shown as a color-coded lookup in 3D relief. Simulated cleft glutamate concentrations (black), AMPAR current (red), and NMDAR current (blue) are shown up to the clip time point. Right panels, The same but during delayed fusion pore opening. Receptor colors are dependent on state (see Fig. 7*D*). The still is of the video 11.19 ms after the start of fusion. [View online]

To investigate the effects of $GABA_B$ and 5-HT_{1B} receptors on neurotransmitter release, we whole-cell voltage-clamped subicular pyramidal neurons (Fig. 1*A*) and stimulated CA1 axons with glass-coated tungsten microelectrodes at low intensity to ensure focal stimulation (5-20 µA, 200 µs). Recorded events were of low amplitude (Fig. 1*B*): ~10 times the unitary amplitude determined from spontaneous release in TTX shown in earlier work (Hamid et al., 2014), which ensured that responses were monosynaptic. To prevent polysynaptic firing by recurrent excitation of CA1 neurons, the tissue was cut at the CA1-subicular boundary. We recorded responses in bicuculline (5 μM) and 2-amino-5-phosphonopentanoic acid (AP5, 50 μM) to isolate AMPAR-mediated currents. We applied the selective 5-HT_{1B} receptor agonist CP93129. Effects of a saturating concentration (1 μM) and at a concentration approximately the EC_{50} (50 nM) are shown (for the concentration response, see Fig. 1*Ba*,*Da*). CP93129 reduced the EPSC peak amplitude to 19.6 ± 3.9% at a saturating dose (1 μM, $n = 8$; $EC_{50} = 0.033 \pm 0.04$ μM). These EPSCs are also inhibited by the $GABA_B$ receptor agonist baclofen to 7.2 ± 2.3% of control (100 μM baclofen, $n = 5$, $EC_{50} = 0.35 \pm 0.18$ μM) (Fig. 1*Bb*,*Db*).

We have previously shown that 5-HT_{1B} receptors target G$\beta\gamma$ to SNARE complexes in CA1 terminals (Hamid et al., 2014), and G$\beta\gamma$ competes with Ca^{2+}-synaptotagmin binding to SNARE complexes. In lamprey, this may confer Ca^{2+} dependency on inhibition (Yoon et al., 2007). To test for this in CA1 subicular synapses, we recorded EPSCs in HEPES buffered Ringer (to prevent Ca^{2+} precipitation). Increasing $CaCl_2$ concentrations (10 mM) enhanced the EPSC (Fig. 1*Ca*,*Cb*), but CP93129 now caused significantly less inhibition (Fig. 1*Cb*,*Da*; at 50 nM, paired Student's *t* test, $t_{(15)} = 6.00$, $p = 0.00001$, $n = 13$ and $n = 8$; and at 400 nM $t_{(4)} = 2.46$, $p = 0.03$, $n = 10$ and $n = 4$). The EC_{50} of CP93129 increased from 33 ± 4 nM to 320 ± 19 nM. In contrast, baclofen (600 nM) inhibition was unaffected by high Ca^{2+} concentration ($t_{(16)} = 0.88$, $p = 0.38$; Fig. 1*Cc*,*Db*). This latter result implies that 10 mM Ca^{2+} does not cause saturating Ca^{2+} entry with respect to neurotransmitter release, allowing reduced Ca^{2+} entry by baclofen to reduce P_r.

Paired-pulse ratios are modified by $GABA_B$ receptors but not by 5-HT_{1B}

Colocalized $GABA_B$ and 5-HT_{1B} receptors act at different targets, Ca^{2+} channels or the SNARE complex, respectively; therefore, their activation may evoke different effects on vesicle fusion. We measured paired-pulse ratios (PPRs) to determine whether these receptors cause inhibition by a change in P_r (Dobrunz and Stevens, 1997). As a control, we raised the extracellular Mg^{2+} concentration (Del Castillo and Katz, 1954) from 1 to 4 mM to reduce presynaptic Ca^{2+} entry and therefore P_r. In 4 mM Mg^{2+}, the mean amplitude of the first EPSC was reduced (to 42 ± 3% of control $n = 14$; Fig. 2*A*), and the PPR (EPSC2/EPSC1) was increased by a factor of 1.64 ± 0.09, $n = 14$ (quantified in Fig. 2*E*, red) demonstrating a Ca^{2+}-dependent reduction in P_r.

We inhibited EPSCs with baclofen (600 nM, approximately half-maximal concentration; Fig. 2*B*), which reduced the first EPSC to 40 ± 6% and enhanced PPRs (by 1.62 ± 0.1, $n = 10$; quantified in Fig. 2*E*, green) demonstrating an effect of $GABA_B$ receptors on P_r, consistent with our earlier work showing their effect on presynaptic Ca^{2+} entry (Hamid et al., 2014). The effect on PPR was concentration-dependent (Fig. 2*F*) with a similar concentration response to the effect on EPSC amplitude (Fig. 1*Db*).

As a negative control, AMPAR antagonism with half-maximal concentrations of the glutamate receptor antagonist kynurenate (200 μM) showed no effect on PPRs (Fig. 2*C*). The EPSC2/EPSC1 ratio was 1.13 ± 0.04 ($n = 19$) of control (quantified Fig. 2*E*, gray). This is expected for postsynaptic targets. CP93129 inhibits CA1-subicular EPSCs presynaptically (Zurawski et al., 2019). Nevertheless, we now show a half-maximal CP93129 (50 nM) concentration, which reduced the first EPSC to 54 ± 4% of control, did not alter PPRs (PPR in CP93129 was 1.13 ± 0.07 of control; Fig. 2*D*, *E*, blue; $n = 14$). This lack of effect of CP93129 on PPRs was consistent over the full concentration response range of CP93129 on EPSCs (Fig. 2*G*).

A one-way ANOVA to test effects of raised Mg^{2+} concentration, of baclofen, kynurenate, and of CP93129 on PPRs (data from Fig. 2*E*), showed significance (ANOVA single factor

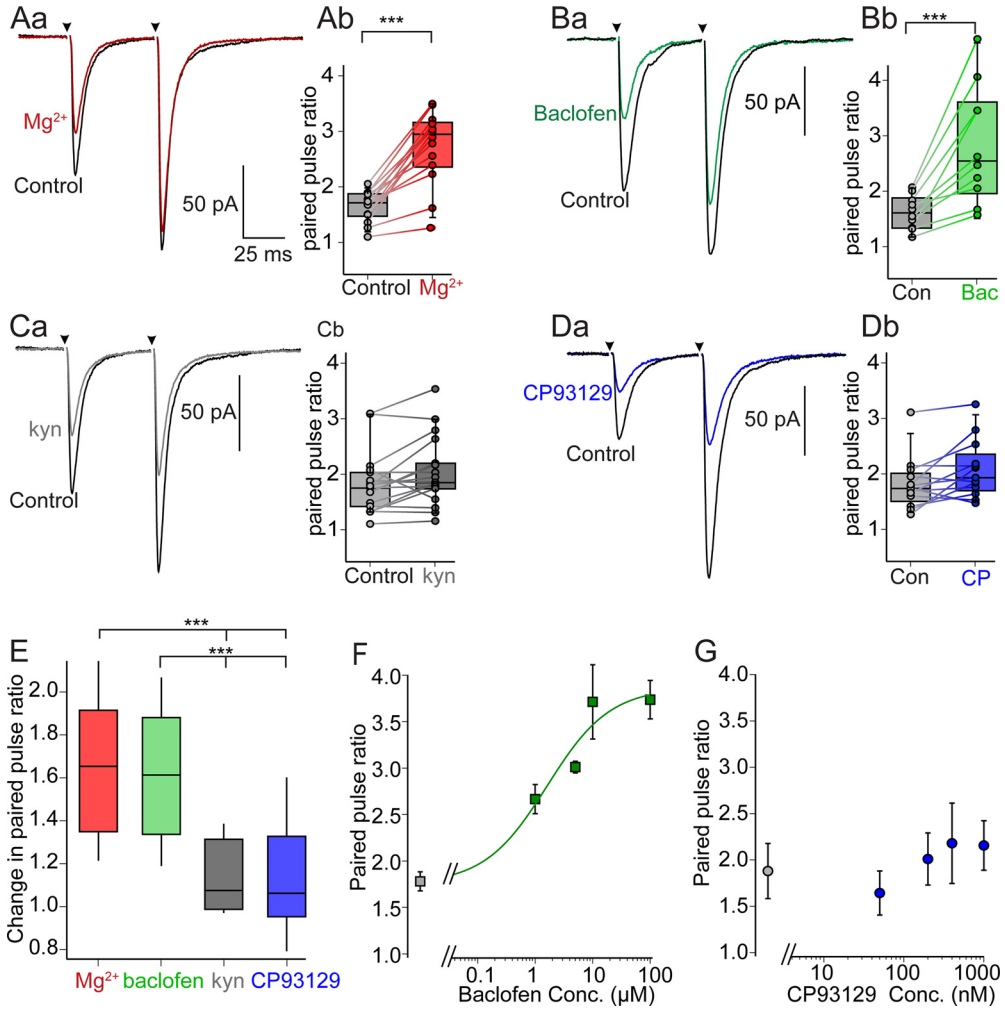

Figure 2. P_r is unaffected by 5-HT_{1B} but reduced by $GABA_B$ receptor activation. ***A***, Paired-pulse stimuli applied to CA1 axons (50 ms intervals). ***Aa***, Means of 10 EPSCs. Extracellular [Mg^{2+}] was raised from 1 to 4 mM to reduce Ca^{2+} entry (red) and thus P_r. This reduced the mean amplitude of the first EPSC more than the second. The effect of high Mg^{2+} on the PPR is quantified to show scatter plots of PPRs in control and high Mg^{2+} for each cell and box plots of the same data (***Ab***). ***B***, A similar experiment but with addition of the $GABA_B$ receptor agonist, baclofen (600 nM). ***Ba***, Mean EPSCs show an increase in PPR quantified in ***Bb*** as for ***Ab***. ***C***, A negative control using a glutamate receptor antagonist, kynurenate (200 μM; gray). This gave no change in PPR (***Ca***, quantified in ***Cb***). ***D***, Similar experiment but with the 5-HT_{1B} receptor agonist, CP93129 (50 nM; blue). This again gave no change in PPR (***Da***, quantified in ***Db***). ***E***, Changes in PPRs normalized to pretreatment controls shown as box plots (1.0 = no change, boxes 25% and 75% with means, whiskers to 10% and 90%) for all recordings in the conditions shown in ***A-D***. ***F***, The effect of baclofen concentration versus normalized PPR was plotted. This is concentration-dependent. ***G***, The effect of CP93129 concentration on PPR was plotted. This was not concentration-dependent. ***$p < 0.001$.

$F_{(3,53)} = 16.85$, $p = 8 \times 10^{-8}$). *Post hoc* Tukey HSD analysis revealed no significant difference between effects of raised Mg^{2+} and baclofen ($p > 0.1$) and none between effects of kynurenate and CP93129 ($p > 0.1$). However, the effect of CP93129 was significantly different from lowering P_r with raised Mg^{2+} ($p < 0.001$) or baclofen ($p < 0.001$). Thus, effects of 5-HT_{1B} receptors are paradoxical, they are presynaptic but do not alter P_r, whereas $GABA_B$ receptors that are also presynaptic do alter P_r.

5-HT_{1B} but not $GABA_B$ receptors enhance low-affinity block of AMPA EPSCs

We investigated whether presynaptic receptors alter synaptic cleft glutamate concentrations at postsynaptic AMPARs. Partial block of EPSCs by a low-affinity antagonist is caused by antagonist binding and unbinding. If the antagonist unbinds within the time course of glutamate in the synapse, antagonist bound receptors will then become available for either glutamate or antagonist binding. Therefore, fractional low-affinity antagonism of the AMPAR EPSC will depend on the glutamate concentration (Clements et al., 1992). EPSCs evoked by low glutamate cleft concentrations will be more completely antagonized than those at high concentrations.

To first determine any effect of a reduction in P_r on cleft glutamate concentration, we recorded AMPAR EPSCs. The effect of lowering P_r with high Mg^{2+} was tested against the efficacy of low-affinity kynurenate antagonism. We compared kynurenate efficacy in control (1 mM) and high (4 mM) Mg^{2+} concentrations in the same cell and stimulus intensity because it is not clear that the mean control cleft glutamate concentrations were identical from cell to cell. After obtaining baseline EPSCs, we superfused the slice with kynurenate (200 μM) to obtain a partial block of the EPSC (in the example to 70% of control; Fig. 3*Aa*, gray). Kynurenate was removed to remeasure control EPSCs. The Mg^{2+} concentration was then increased to 4 mM to reduce P_r (EPSC reduced to 69% of control, Fig. 3*Aa*, red). Kynurenate (200 μM) was reapplied in 4 mM Mg^{2+} to measure its efficacy at a lower P_r. The EPSC in 4 mM Mg^{2+} was reduced by the same

proportion as in control (to 67% of response in 4 mM Mg^{2+}; Fig. 3*Aa*, purple). To compare inhibition by kynurenate in control and 4 mM Mg^{2+} the responses in 4 mM Mg^{2+} alone and combined with kynurenate were scaled to control amplitudes (Fig. 3*Ab*) showing similar proportionate inhibition. In repeat experiments, the drug sequence was randomized. For all cells, in 1 mM Mg^{2+}, kynurenate (200 μM) reduced EPSCs to 44 ± 4% of control; and in 4 mM Mg^{2+}, kynurenate similarly reduced the EPSC to a not significantly different 43 ± 4% ($n = 10$; Fig. 3*Ac*, purple; paired Student's *t* test, $t_{(9)} = 0.39$, $p = 0.7$).

We then assayed the efficacy of kynurenate inhibition before and in baclofen which will also alter P_r. In the example, kynurenate (200 μM) reduced the mean EPSC amplitude to 62% of control (Fig. 3*Ba*, gray). In baclofen (600 nM; Fig. 3*Ba*, green), the inhibited EPSC was reprobed with kynurenate (200 μM), which now reduced the EPSC to 61% of its amplitude in baclofen alone (Fig. 3*Ba*, dark green). Responses were again scaled to compare the effect of kynurenate in controls and in baclofen (Fig. 3*Bb*). In 19 experiments, kynurenate inhibited control responses to 46 ± 3% and the inhibitory effect was slightly but significantly less in baclofen, inhibiting to 51 ± 3% (Fig. 3*Bc*; green; paired Student's *t* test, $t_{(18)} = 2.19$, $p = 0.04$).

We similarly assayed the efficacy of kynurenate block before and in CP93129, which did not alter P_r. In the example, kynurenate (200 μM) reduced the peak EPSC amplitude to 55% of control (Fig. 3*Ca*, gray). After removal of kynurenate, EPSC amplitudes were recorded to reconfirm control responses. CP93129 (50 nM) was applied (Fig. 3*Ca*, light blue), and the CP93129 inhibited EPSC was reprobed with kynurenate (200 μM), which now reduced the EPSC to 38% of its amplitude in CP93129 alone (Fig. 3*Ca*, blue). Responses were again scaled to directly compare the effect of kynurenate in controls and in CP93129 showing an enhancement in inhibition (Fig. 3*Cb*). In 17 experiments, kynurenate inhibited control responses to 57 ± 3% and responses in CP93129 to 37 ± 2%. This latter inhibitory effect was significantly greater than the effect of kynurenate alone (Fig. 3*Cc*; paired Student's *t* test, $t_{(16)} = 5.56$, $p = 2.1 \times 10^{-5}$).

As a negative control for the effect of CP93129 in kynurenate, we replaced the competitive antagonist (kynurenate) with a noncompetitive AMPAR antagonist, GYKI52466 (GYKI). GYKI should inhibit EPSCs similarly, regardless of glutamate concentration because it does not compete with glutamate (Fig. 3*D*). Mean inhibition by GYKI in control was to 63 ± 4%, and the efficacy of GYKI was slightly but significantly reduced in CP93129 ($n = 6$, to 68 ± 4% of response in CP93129, paired Student's *t* test, $t_{(5)} = 3.85$, $p = 0.011$). This result is small but may imply a slight bias in analysis recordings of EPSC amplitudes as their amplitude is reduced to very small values by combined ligands. Recording noise may contribute slightly to the computed result because the EPSC measurement algorithm searched for a smoothed positive maximum. Thus, in very small or results with a failure, there may be a small positive bias in the result. The result may indicate that we have slightly underestimated the effect of 5-HT_{1B} receptors on cleft glutamate concentrations, but does not change the conclusion. This bias may also underlie the slight but not significant relative reduction in effect of kynurenate seen in baclofen (Fig. 3*Bc*).

The effects of high Mg^{2+}, baclofen, and CP93129 on the efficacy of kynurenate and the effect of CP93129 on the efficacy of GYKI on the inhibition of the synaptic responses were compared with one another by comparing the ratios of effects of antagonist (kynurenate or GYKI) with the same antagonist combined with either 4 mM Mg^{2+}, with baclofen, or with CP93129 (Fig. 3*E*). All four experiments were compared with a one-way ANOVA showing substantial significance ($F_{(3,48)} = 15.88$, $p = 1.4 \times 10^{-6}$). *Post hoc* Tukey's HSD analysis revealed that the effect of baclofen was not significantly different from the effect of high Mg^{2+} on the efficacy of kynurenate inhibition ($p > 0.1$). This is consistent with inhibition mediated by a change in P_r of univesicular events at each synapse. In contrast, the effect of CP93129 on kynurenate-mediated inhibition was significantly greater than that of Mg^{2+} ($p < 0.005$), baclofen ($p < 0.001$), and of the effect of CP93129 on GYKI inhibition ($p < 0.005$).

Single raised concentrations of Mg^{2+} (4 mM) or single concentrations of baclofen (600 nM), or CP93129 (50 nM) show varying degrees of inhibition from cell to cell. For example, initial effects of 50 nM CP93129 reduced the EPSC from as little as 0.8 of control to as much as 0.3. If this variance reflects the efficacy of the agonist on cleft glutamate concentration, it will correlate with amplification of agonist inhibition by kynurenate (shown in Fig. 3*E*). To test this, we compared the efficacy of the agonist alone in each neuron (agonist/control), to the change in agonist efficacy by kynurenate [(kynurenate/control)/(agonist/kynurenate + agonist)]. We first plotted these for effects of high Mg^{2+} (Fig. 3*F*). There was no correlation between inhibition by 4 mM Mg^{2+} with the subsequent effect of Mg^{2+} on kynurenate inhibition. This is consistent with a Mg^{2+}-induced change in P_r at univesicular synapses causing no change in cleft glutamate concentration regardless of the initial efficacy of raised Mg^{2+}. Similarly, there is no correlation between the efficacy of baclofen and its effect on subsequent kynurenate block (Fig. 3*G*). However, there is a strong correlation between the CP93129 efficacy and its amplification of kynurenate inhibition (Fig. 3*H*), indicating that the greater the effect of presynaptic 5-HT_{1B} receptors, the lower it drives cleft glutamate concentration and therefore the larger inhibitory effect of kynurenate. We conclude that at CA1 presynaptic terminals changes in P_r do not alter cleft glutamate concentrations, but 5-HT_{1B} receptors do.

It was important to determine that synaptic responses were not impacted by changes in whole-cell recording access during the experiments. In all experiments, we monitored whole-cell access by applying a small (5 mV, 20 ms) test pulse before each evoked EPSC was recorded. An example is shown of this recording throughout a sequential application of kynurenate, and CP93129; and then the drugs combined simultaneously measuring effects on synaptic responses (Fig. 4*A*,*B*), while simultaneously monitoring whole-cell series resistance calculated from double exponentials fitted to the settling of the step current (Fig. 4*C*). Experiments were terminated and data not used if access resistance changed by >20%. For the examples used for analysis (Fig. 4*D*), no significant difference was seen for access impedance (ANOVA single factor $F_{(3,64)} = 0.065$, $p = 0.97$) or holding current ($F_{(3,64)} = 0.18$, $p = 0.91$) when comparing between periods of ligand applications.

5-HT_{1B} but not $GABA_B$ receptors differentially inhibit AMPA and NMDA EPSCs

Glutamate activates receptors with varying sensitivities: for example, AMPA, NMDA, and metabotropic glutamate receptors have different affinities for glutamate and different numbers of glutamate binding sites. Consequently, changes in cleft glutamate concentration may differentially alter their activation (Choi et al., 2003; Schwartz et al., 2007; Gerachshenko et al., 2009). We compared 5-HT_{1B} and $GABA_B$ receptor inhibition on AMPAR- and

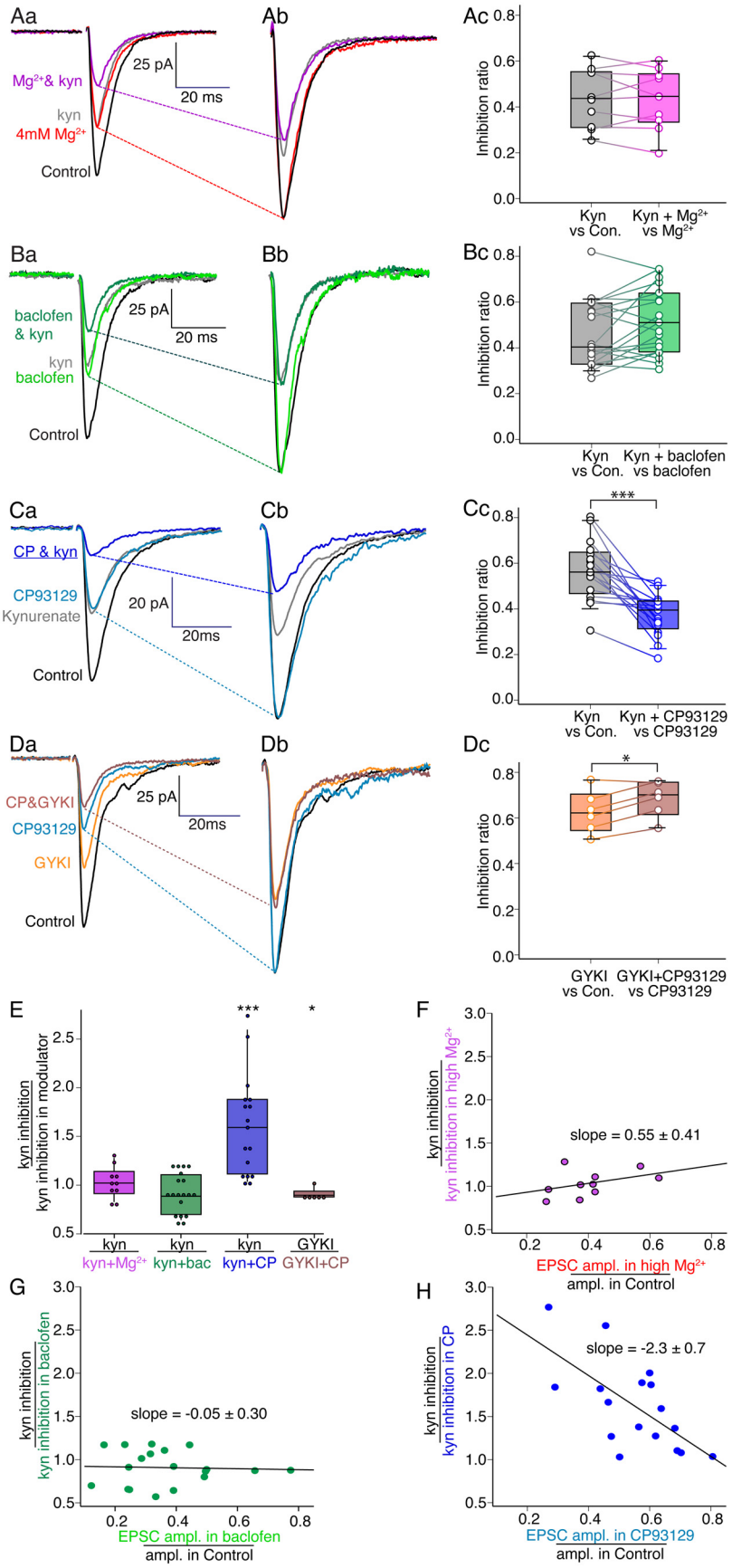

Figure 3. 5-HT_{1B} but not $GABA_B$ receptors increase the potency of a low-affinity AMPAR antagonist-mediated block of EPSCs. ***A***, Effect of raised Mg^{2+} on EPSC inhibition by a low-affinity competitive antagonist, kynurenate. ***Aa***, Kynurenate (200 μM; gray) partially inhibited EPSCs, shown as means of 10 traces. After kynurenate wash, 4 mM Mg^{2+} (red), to decrease P_r reduced EPSCs. Kynurenate 200 μM was then combined with high [Mg^{2+}] (purple). ***Ab***, For clarity, traces in 4 mM Mg^{2+} scaled to control. ***Ac***, Kynurenate inhibited EPSCs to a similar ratio in control and 4 mm Mg^{2+}. Inhibition ratios plotted and overlaid on boxplots (boxes 25% and 75% with means, whiskers to 10% and 90%). ***Ba***, Kynurenate (200 μM; gray) reduced EPSCs. After kynurenate wash, baclofen (600 nM; light green) reduced the EPSC. Kynurenate (200 μM) with baclofen (600 nM; dark green) reduced the EPSC similarly to baclofen alone. ***Bb***, Reponses in baclofen scaled as for ***Ab***. ***Bc***, Data from all cells. ***Ca***, Kynurenate (200 μM; gray) reduced EPSCs. After wash, CP93129 (50 nM; light blue) reduced the EPSC. Kynurenate (200 μM) with 50 nM CP93129 (blue) reduced the EPSC to a greater proportion than CP93129 alone. ***Cb***, Reponses in CP93129 scaled as for ***Ab***. ***Cc***, Data from all cells. ***D***, Noncompetitive AMPAR antagonist GYKI used as control. ***Da***, GYKI (10 μM; orange) reduced EPSCs. After wash, CP93129 (50 nM) inhibited EPSCs (blue). Coapplication of 10 μM GYKI with 50 nM CP93129 (pink) reduced EPSCs as controls. ***Db***, Responses in CP93129 scaled as above. ***Dc***, Data from all cells. ***E***, Box plots overlaid with individual cell data comparing ratio of inhibition by kynurenate or GYKI alone, to inhibition in kynurenate plus high Mg^{2+} (pink), baclofen (green), or CP93129 (blue) or to GYKI and CP93129 (brown). A value of 1 indicates the modulatory agonist had no effect on kynurenate or GYKI potency; higher values show enhanced potency. ***F***, Change in kynurenate inhibition caused by 4 mM Mg^{2+} (data from ***A***) plotted against initial efficacy of 4 mM Mg^{2+} for each neuron. The slope was indistinguishable from zero. ***G***, Similar effect by baclofen on kynurenate inhibition (***B***) plotted against initial efficacy of baclofen in each neuron. Slope was again indistinguishable from zero. ***H***, Change in kynurenate inhibition by CP93129 (***C***) plotted against the initial efficacy of CP93129 in each neuron. Slope (−2.3) showed correlation ($R^2 = 0.4$). *$p < 0.05$. ***$p < 0.001$.

NMDAR-mediated synaptic responses. AMPAR-mediated EPSCs were recorded as before. We recorded NMDAR-mediated synaptic responses in bicuculline (5 μM), and NBQX (5 μM) at a holding potential of −35 mV. Baclofen (600 nM) equally inhibited AMPA and NMDA components of EPSCs (Fig. 5*A*; to 49 ± 6%, $n = 8$, and to 54 ± 4%, $n = 6$, respectively; $t_{(12)} = 0.80$, $p = 0.44$). CP93129 (50 nM) inhibited AMPA EPSCs significantly more than NMDA EPSCs (Fig. 5*B*; to 54 ± 6%, $n = 10$, and to 93 ± 4%, $n = 6$, respectively; $t_{(14)} = 7.15$, $p = 4.9 \times 10^{-6}$). Concentration response curves of CP93129 inhibition of AMPA and NMDA EPSCs diverged (Fig. 5*C*). AMPAR-mediated EPSCs were maximally inhibited to 20 ± 3% of control, whereas NMDAR-mediated EPSCs were significantly less inhibited to 75 ± 6% (paired Student's t test, $t_{(7)} = 6.48$, $p = 0.00017$). We obtained similar results when we recorded NMDA and AMPA EPSCs simultaneously from the same synapses. AMPAR- and NMDAR-mediated responses were recorded simultaneously by holding the membrane potential at positive values and recording events early in the response or later. We measured AMPAR EPSC amplitudes within 2 ms

of stimulation, whereas NMDA responses were measured during the decay after 100 ms (Fig. 5*D*) because these receptors show much slower decay kinetics than AMPAR-mediated responses (Lester et al., 1990). In control conditions with no drugs, NMDAR EPSC amplitudes covary with those of AMPARs (Fig. 5*E*), indicating that the receptors are activated on the same synapses. In 6 neurons, we plotted the mean amplitudes of AMPAR- and NMDAR-mediated EPSCs with increasing doses of CP93129. AMPAR EPSCs were inhibited to a significantly greater extent than were NMDAR EPSCs at all applied concentrations of CP93129 (Fig. 5*F*). For the approximate half-maximal concentration (50 nM) $t_{(5)} = 5.61$, $p = 0.002$) and for the maximal concentration (1000 nM) $t_{(5)} = 7.52$, $p = 0.0007$).

If the lack of effect of CP93129 on NMDA EPSCs is because it causes reduced cleft glutamate concentrations, then an effect of CP93129 would be revealed by low-affinity NMDAR antagonists that will amplify effects of changing glutamate concentrations at NMDARs (Choi et al., 2000). We recorded evoked pharmacologically isolated NMDAR EPSCs ($n = 6$) at 50 mV in bicuculline (5 μM) and NBQX (5 μM). Low doses of CP93129 (10 and 50 nM) did not significantly reduce the EPSC in 6 neurons (ANOVA single factor $F_{(2,12)} = 3.80$, $p = 0.052$; Fig. 5*Ga*,*H*). In a further 6 neurons, the same experiment was performed in the low-affinity competitive NMDAR antagonist L-5-amino pentanoic acid (L-AP5, 250 μM). The EPSC was reduced to 55 ± 4% of control by L-AP5 (Fig. 5*Gb*,*H*). In L-AP5, CP93129 at both 10 and 50 nM CP93129 now inhibited these partially blocked EPSCs to 66 ± 7 and 45 ± 4% of the response in L-AP5 alone. These reductions were significant (ANOVA single factor $F_{(2,12)} = 7.22$, $p = 0.009$). Thus, NMDARs are exposed to a similar 5-HT_{1B} receptor-mediated reduction in glutamate concentration to that seen by AMPARs.

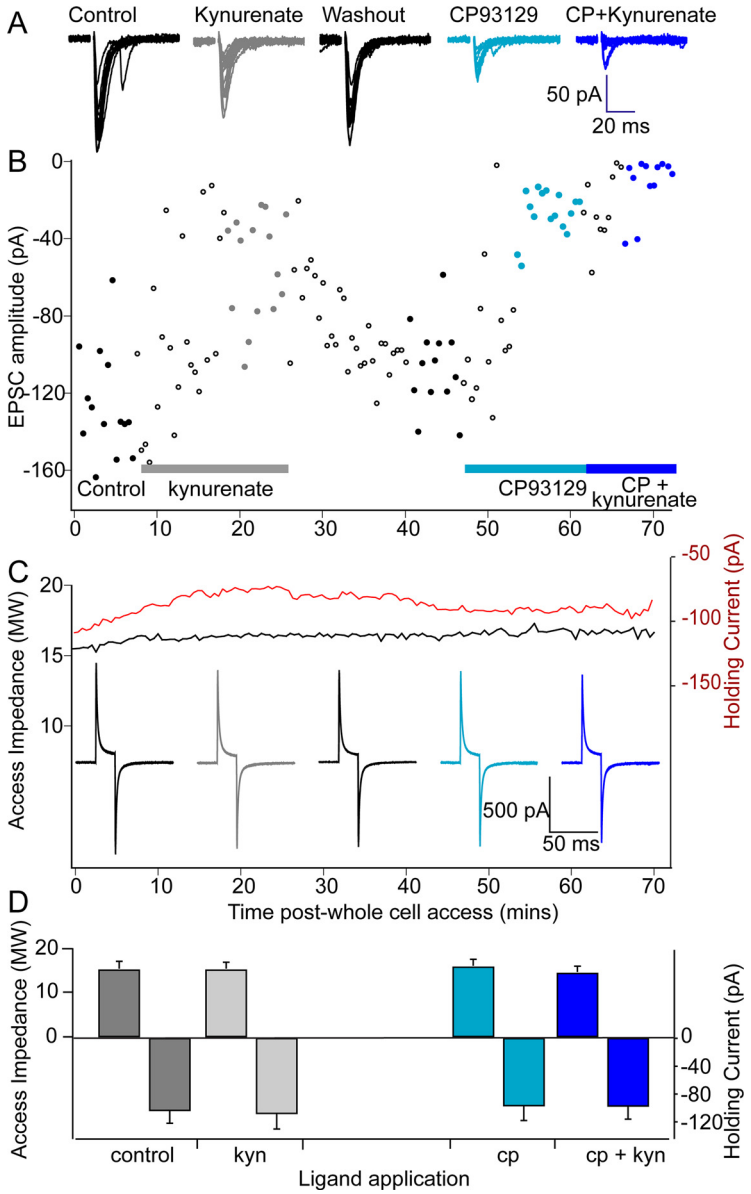

Figure 4. Stability of recording access. ***A***, Sequential recordings of evoked AMPAR-mediated EPSCs during recording through each drug condition to show recording stability. Individual EPSCs are shown for one recording in which the effects of CP93129 and its amplification by kynurenate were tested. ***B***, Graph of peak amplitudes of all EPSCs recorded. Closed circles represent measured responses corresponding to the EPSCs shown in ***A***. Open circles during wash in or washout of the drugs were not measured. Colors correspond to EPSCs in ***A***. ***C***, Graphs represent whole-cell access impedance (black), and holding current (red) throughout the experiment. Whole-cell access impedances (R_a) were calculated from double exponentials fit to the decays from small depolarizing current steps applied before each EPSC was stimulated (Sigworth, 1983). Example responses to voltage steps at each drug application are shown. Color the same as for ***A***. ***D***, From all cells, histograms represent mean ± SEM for access impedance (positive bars) and holding currents (negative bars) during control, application of kynurenate, CP93129, and kynurenate + CP93129. Colors during ligand applications are the same throughout the figure.

The effect of 5-HT_{1B} receptors on glutamate release

It is possible to image glutamate release using genetically engineered glutamate sensors. To achieve this, we virally infected subicular neurons with iGluSnFR using an AAV1 containing iGluSnFR.WPRE.SV40 under a human synapsin promotor (pAAV.hSyn.iGluSnFr.WPRE.SV40 (AAV5) (Marvin et al., 2013) by injecting the viral vector into hippocampi of 22 d rats . In hippocampal slices from these animals, epifluorescence imaging (excitation 470 nm, emission, 520 nm) revealed fluorescent subicular pyramidal neurons. The slices were placed in a custom-designed imaging chamber and a stimulation electrode placed as for electrophysiological recording. The subicular region was then imaged using LLSM (Fig. 6*A*). The light sheet penetrated to ~50 μm in the slice, and time-series images of single planes (512 × 512 pixels; 52 × 52 μm) were captured with a single exposure time of 10 ms and a frame rate of 80 Hz. Stimuli were applied to CA1 axons at 5 s intervals to evoke events that appeared stochastically located, varying from stimulus to stimulus across the FOV (Fig. 6*B*). Repeated stimuli revealed multiple locations of release that were resolved over a sequence of up to 21 individual stimuli. Events were well resolved using LLSM imaging (Fig. 6*C*,*D*).

We tested the effect of 5-HT_{1B} receptor activation on these evoked fluorescence transients by recording events at single sites during repeated stimuli before and after application of

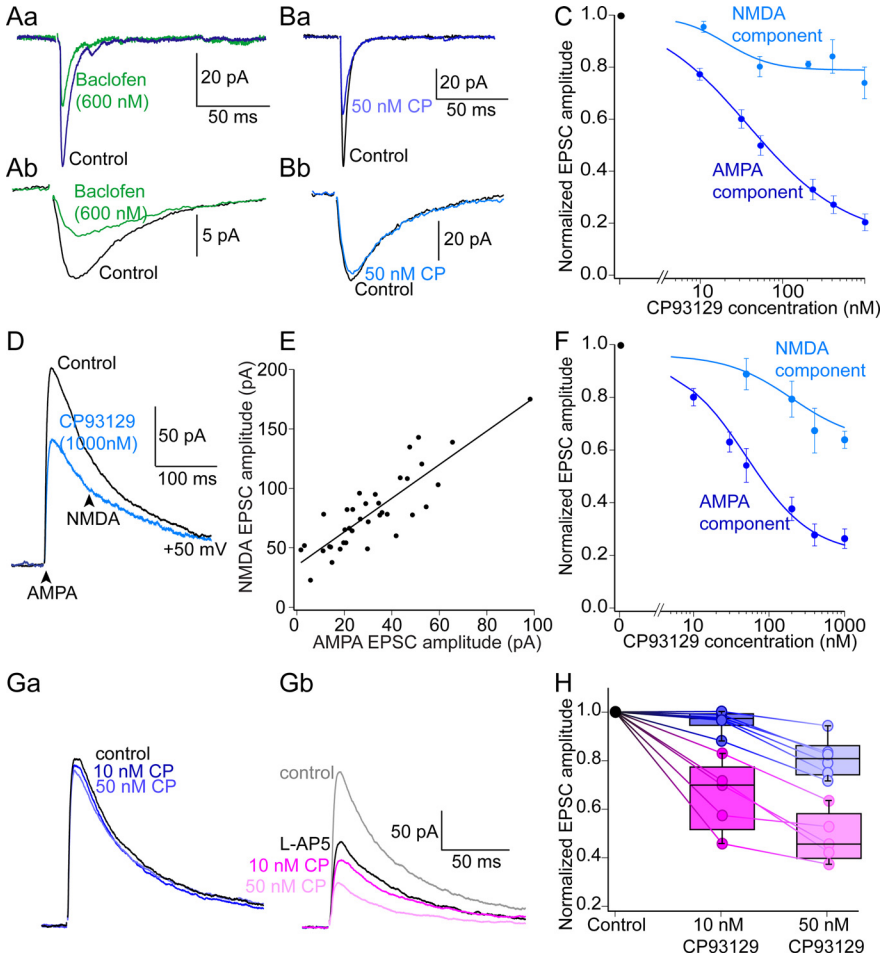

Figure 5. Differential inhibition of AMPAR- and NMDAR-mediated EPSCs. ***A***, In separate recordings AMPA-mediated EPSCs were recorded in D-AP5 (***Aa***) and NMDA-mediated EPSCs in NBQX (***Ab***). Baclofen (600 nM; green) similarly inhibited both of these responses. ***B***, Similar recordings were made but CP93129 (***Ba***, 50 nM; blue) inhibited the AMPAR-mediated EPSC, but not the NMDAR-mediated EPSC (***Bb***, light blue). ***C***, Concentration response effects of CP93129 versus the AMPAR (blue) and NMDAR EPSCs (light blue) show a large difference in efficacy. ***D***, The differential effect of CP93129 on AMPAR and NMDAR responses is found at the same synapses. Compound EPSCs without glutamate receptor antagonists recorded at a holding potential of 50 mV. Early responses (2 ms after stimulus) are dominated by AMPARs (bottom arrow), late responses (100 ms after stimulus) by NMDARs. CP93129 at a saturating dose (1 μM) was applied (blue). ***E***, For individual recordings, sequential response amplitudes of AMPA and NMDA responses were plotted against each other. These responses covaried, indicating that they colocalize to the same synapses. ***F***, Mean amplitudes of AMPAR- and NMDAR-mediated EPSCs during the same stimuli plotted with increasing concentrations of CP93129. AMPAR EPSCs were inhibited to a greater extent than were NMDAR EPSCs. ***G***, CP93129-mediated inhibition of the NMDA component is amplified by the low-affinity competitive antagonist (L-AP5). In control experiments (***Ga***), 10 and 50 nM CP93129 (blue) had little effect on isolated NMDA-mediated EPSC (recorded at 50 mV in NBQX and bicuculline). L-AP5 (250 μM) partially inhibited this response (***Gb***, black). This inhibited response was now substantially inhibited by 10 and 50 nM CP94129 (red and pink). ***H***, Quantitation of the data from ***G***, showing inhibition by CP93129 in control (blue, normalized to precontrol recordings) and after treatment with L-AP5 (pink, normalized to recordings in L-AP5 alone.

CP93129 (100 nm). Frequency of events was calculated by whether an event was recorded on stimulation or not. The probability of recording an event at the same location as in control was unchanged in CP93129 0.20 ± 0.02 versus 0.19 ± 0.03 in control (Fig. 6*F*; $t_{(12)} = 0.17$, $p = 0.87$). Similar recordings were made before and during baclofen (1 μM) application. In these recordings, the probability of recording events was reduced significantly from 0.29 ± 0.07 in control to 0.08 ± 0.05 in baclofen ($t_{(8)} = 4.24$, $p = 0.0014$).

We also measured effects of agonist application on event amplitude. However, event frequencies on single stimuli were low. To increase event frequency, stimuli were applied as paired pulses at 100 ms intervals, and all poststimulation peak fluorescence transient amplitudes were determined as ΔF/F calculated from the ratio of peak response to amplitude immediately before the stimulus after background subtraction of fluorescence adjacent to the ROI. Data were captured for each of every 24 stimuli at 5 release locations located in 3 slices for application of CP93129 and for 5 locations in 4 slices for baclofen. Event amplitudes were plotted as frequency histograms. An example is given for baseline and in CP93129 (Fig. 6*G*, top). In baseline conditions, events largely fell into either failures, with mean signal similar to background noise, or into a signal centered on a recurring amplitude (quantum). Some larger events were also recorded. CP93129 (100 nM, blue) caused this dual amplitude distribution to be lost. Mean effects of CP93129 were compared for all 5 locations with amplitudes normalized to the mean value of a single quantum in baseline conditions (Fig. 6*G*, bottom). The distinction between failures and a single quantum value was lost in CP93129, but there was no significant change in the number of observed failures ($t_{(4)} = 1.2$, $p = 0.15$). This is emphasized by plotting a multiple Gaussian curve to the baseline data with the constraints that sequential quantal events amplitudes and widths increased as integer multiples of the quantal amplitude.

Similar experiments were performed in baseline, then baclofen (Fig. 6*H*, green). In contrast, baclofen (1 μM) significantly increased the incidence of failures ($t_{(4)} = 5.28$, $p = 0.003$), but remaining event amplitudes fell into the same amplitude bins as baseline responses. This is emphasized by multiple Gaussian fits to baseline results and from events in baclofen in which the single event amplitude calculated from these fits was not significantly altered ($t_{(4)} = 1.7$, $p = 0.16$), whereas both the number of failures ($t_{(4)} = 2.9$, $p = 0.04$) and the number of single quantum events ($t_{(4)} = 4.0$, $p = 0.02$) were. We also measured the decay kinetics of the responses in baseline and in both agonists, but no changes were measured. This is likely because of the relatively high affinities of the iGluSnFr variant used such that unbinding of glutamate from the sensor dominates the signal off rate. Indeed, the size of the events compared with the point spread function of the microscope (Fig. 6*I*), which demonstrate submicron resolution, indicates that we detect glutamate spillover from the synapse as a large part of the signal.

Simulating glutamate release and receptor activation

$GABA_B$ receptors reduce P_r, whereas 5-HT_{1B} receptors lower cleft glutamate concentrations. The latter may be because of a modification of the fusion pore during neurotransmitter release

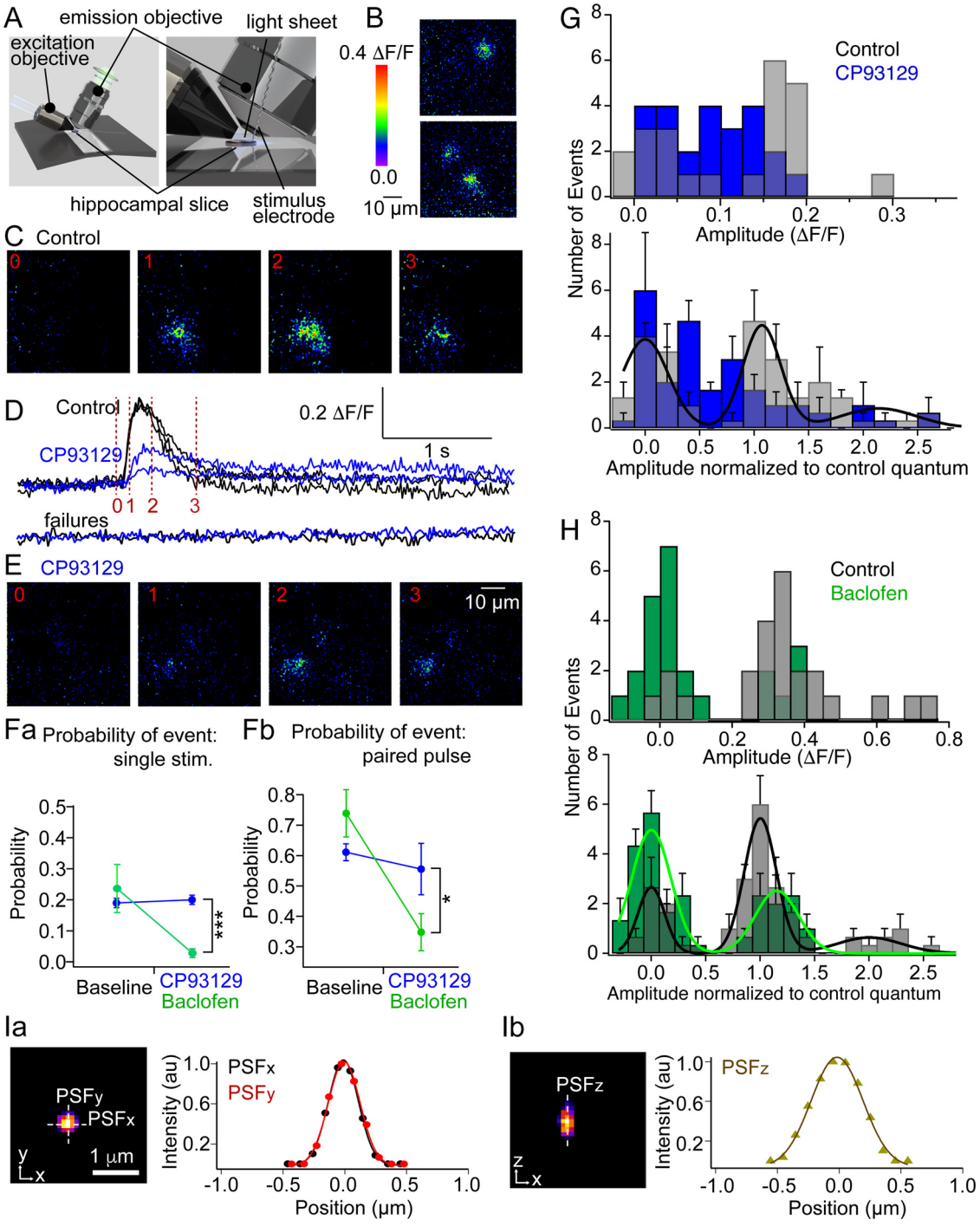

Figure 6. Imaging evoked glutamate release with iGluSnFR. ***A***, Imaging of iGluSnFr expressed in subicular neurons was performed under LLSM adapted to allow recording and stimulation of hippocampal slices. The schematic shows the arrangement of preparation and lenses. ***B***, While imaging labeled subicular pyramidal neurons dendrites, repeated stimulation (1 shock at 5 s intervals) caused stochastic fluorescent transients in subiculum. Shown are 3 responses from 2 separate stimuli. ***C***, Evoked transients recorded in one *z* plane at imaged at 80 Hz expanded from a spot to larger diameter (5-10 μm diameter) objects (time point noted in ***D***, red). ***D***, Transient amplitudes and time courses were calculated from a 5-μm-diameter ROI over the transients. Shown are three control responses at the same location, obtained from 14 stimuli (black). Application of CP93129 (100 nM) reduced the amplitude of the transients that were recorded. Two such responses were recorded in the 14 stimuli in this case (blue). Examples of a failure to evoke a response in control conditions (black) and similarly in CP93129 (100 nm) (blue). ***E***, Example of evoked transient (same location as in ***C***, recorded in CP93129, 100 nM). ***Fa***, CP93129 (100 nM, blue) caused no change in the probability of recording events at the same location over 21 stimuli. In contrast, baclofen (1 μM, green) significantly reduced the probability of recording and event. A two-way ANOVA revealed significance between effects of baclofen and CP93129 ($F_{(1,16)} = 16.1$, $p = 0.001$). Events were determined to be failures if the amplitude after stimulation at that location did not exceed noise. ***Fb***, During paired pulses, overall probability of recording events rose. CP93129 (100 nM, blue) again caused no reduction in probability, whereas baclofen (1 μM, green) did. A two-way ANOVA revealed significance between effects of baclofen and CP93129 ($F_{(1,32)} = 7.12$, $p = 0.011$). ***G***, All evoked event amplitudes were measured and displayed as event/frequency histograms. Under baseline conditions, events were distributed into distinct amplitudes (gray). CP93129 (100 nM, blue) removed this distinction. Top, Histogram example. Bottom, Mean results from five locations normalized to the first baseline event amplitude distinct from noise. Gaussian curves were fitted to baseline data with the constraint that the amplitude and width of non-zero peaks scaled with the number of peaks. This showed a difference in control data between no response and one quantal size. Gaussian fit to the data in CP93129 was not possible. ***H***, Similar experiment with baclofen. Top, Histogram example. Bottom, Average of 5 locations, before and after baclofen (1 μM, green). Baclofen left recorded amplitude of events unaffected but reduced their probability. Mean data in both control (black) and

(Harata et al., 2006; Photowala et al., 2006), changes in MVR (Rudolph et al., 2015), or modulation of the location of release with respect to postsynaptic receptors (Tang et al., 2016; H. Chen et al., 2018; Haas et al., 2018). We created a Monte Carlo simulation of a simple synapse using MCell to probe these possibilities.

The simulated synapse comprised a disk-shaped synaptic cleft, 300 nm in diameter and 20 nm deep, with kinetically modeled AMPARs (Robert and Howe, 2003) and NMDARs (Banke and Traynelis, 2003) placed on the postsynaptic surface (Fig. 7). For each condition, 20 random seeds were simulated, whereby glutamate release was modeled from between one and three vesicles attached to the presynaptic surface with a dynamically opening pore (Movie 1), initially with a 0.4 nm diameter and the length of two lipid bilayers. This is approximately the value proposed for the conductance of foot events in large dense core vesicles (Vardjan et al., 2007). The simulated pore then expanded to the full diameter of the vesicle over a range of time courses from 0.2 to 20 ms. We tested three hypotheses: (1) glutamate release was slowed through a fusion pore; (2) multivesicular vesicle numbers were reduced; and (3) relative locations of release sites and receptors were altered. The parameter files for these simulations are available on our website (https://alford.lab.uic.edu/GPCRs.html). The individual parameters and sources are listed in Table 1.

To simulate a slowly opening fusion pore, the vesicle (containing 5000 glutamates) was attached to the presynaptic membrane through a pore (Fig. 7*A*). The simulated pore expanded to the diameter of the vesicle, but arrested at a diameter of 0.4, 0.5, 0.75, 1.0, 1.5, or 2 nm for 20 ms. Receptors were randomly seeded on the postsynaptic membrane, and their states represented by colors in kinetic models (Fig. 7*D*). Arresting the fusion pore opening at set diameters slowed release and reduced peak cleft glutamate concentrations (Fig. 7*Ab*) compared with full expansion of the pore to the diameter of the vesicle within 200 µs, which represents the default state. This slower glutamate release reduced simulated AMPAR, but not NMDAR, responses (Fig. 7*Ac*,*Ad*) (Movie 2). Both the peak simulated glutamate concentration and peak AMPAR activation were reduced with smaller pore sizes, whereas NMDAR responses remained unchanged (Fig. 7*Ae*,*Af*).

MVR was simulated by varying numbers of simulated fusing vesicles from 1 to 3 (Fig. 7*B*). One vesicle was placed at the center and two offset by 75 nm (Fig. 7*Ba*). Fusion was simulated by pores fully opening in 200 µs. Vesicle content varied from 333 to 5000 glutamates because at high glutamate content the AMPAR response saturated with more than one vesicle, preventing any modulation. Varying vesicle numbers altered cleft glutamate concentration and modulated AMPAR and NMDAR responses nearly equally (Fig. 7*Bb-Bd*). The effect on both NMDARs and AMPARs was modulated by the total number of released glutamates rather than vesicle number (Fig. 7*Be-Bf*).

To vary vesicle fusion position compared with receptors, receptors were seeded within two proscribed areas of the postsynaptic density: one under the fusing vesicle and the other a mean distance of 150 nm away (Fig. 7*Ca*). Release of 5000 glutamates was simulated with complete fusion in 200 µs causing peak glutamate concentrations that differed at the two sites. Little modulation of AMPAR or NMDAR responses occurred (Fig. 7*Cc*,*Cd*). Earlier work simulating vesicles displaced from the release site reported larger effects with fewer released glutamates (Haas et al., 2018). Consequently, the simulation was repeated with 1500 glutamates (Fig. 7*Cf-Ch*). The more distant clusters of AMPAR and NMDAR responses were reduced to 80% and 83% of the amplitude under the release site, respectively. Thus, the response is sensitive to relative locations of vesicle fusion and receptor location, but this effect is small compared with that of experimental 5-HT_{1B} or $GABA_B$ receptor activation and does not recapitulate the difference in effect between AMPAR and NMDAR responses. Overall, changing fusion pore dilation best mimicked the physiological effect of 5-HT_{1B} receptor activation.

Simulating the amplification of inhibition by kynurenate

Experimental effects of the low-affinity antagonist, kynurenate, on AMPAR EPSCs indicate that 5-HT_{1B} receptors, but not $GABA_B$ receptors, lower the concentration of glutamate in the synaptic cleft. To determine whether kynurenate might discriminate between mechanisms by which cleft glutamate concentration is changed based on receptor effects, we simulated the action of kynurenate using a modification of the kinetic model of the AMPAR.

The kinetic model assumed that kynurenate can substitute for glutamate at all states of the receptor but prevented receptor channel opening (Fig. 8*Aa*). Simulations were performed with kynurenate (240 μM) present in the synaptic cleft. This reduced the simulated AMPAR-mediated response to 55% of control (Fig. 8*Ab*). The simulations were then repeated with the synaptic vesicle fusion pore diameter arrested for 20 ms at diameters from 0.4 to 1.5 nm. The effect of kynurenate was enhanced when the pore size was restricted (Fig. 8*B*). The effect of simulated kynurenate was also tested against MVR. Modifying the number of fused vesicles was only effective at a reduced number of glutamates present in each vesicle; thus, these simulations were performed from with three, two, or one vesicles each containing 700 glutamates as for Figure 7*Bb-Bd*. Kynurenate also enhanced the effect of reduced vesicle number on the simulated AMPAR response (Fig. 8*C*).

Effects of both these manipulations were compared with the experimental effects of $GABA_B$ and 5-HT_{1B} receptor activation on AMPA-mediated synaptic responses. Box plots (from Fig. 3*E*) showing CP93129 and baclofen effects on kynurenate-mediated antagonism are presented alongside simulated kynurenate inhibition following a change in number of fusing vesicles (normalized to the maximum, 3) and following arrest of the fusion pore at between 0.4 and 1.5 nm diameters normalized to full fusion (defined as complete opening of the fusion pore the vesicle diameter in 200 µs). Both of these manipulations enhanced the efficacy of kynurenate (Fig. 8*D*).

As for the experimental effects of agonists (Fig. 3*E*,*H*), simulations of variation in inhibition of the AMPA response, either by varying the number of multivesicular fusing vesicles at one active zone (Fig. 8*D*, orange) or varying the vesicle pore diameter (Fig. 8*D*, purple) correlated with the enhancing effect of kynurenate on both manipulations (Fig. 8*E*). Both approaches recapitulated experimental effects of CP93129 but not of baclofen (Fig. 8*E*). From this combination of experimental effects of low-affinity

←

baclofen (green) were fitted with Gaussians with the same constraints as in ***G***. Gaussian fits showing similar quantal peak amplitudes in both conditions. ***I***, Point spread functions (PSFs) of the microscope obtained from a 100-nm-diameter fluorescent bead. ***Ia***, *x*/*y* PSF. ***Ib***, *x*/*z* PSF of the same bead. The bead was embedded 100 µm deep in 1% agarose. $^*p < 0.05$. $^{***}p < 0.001$.

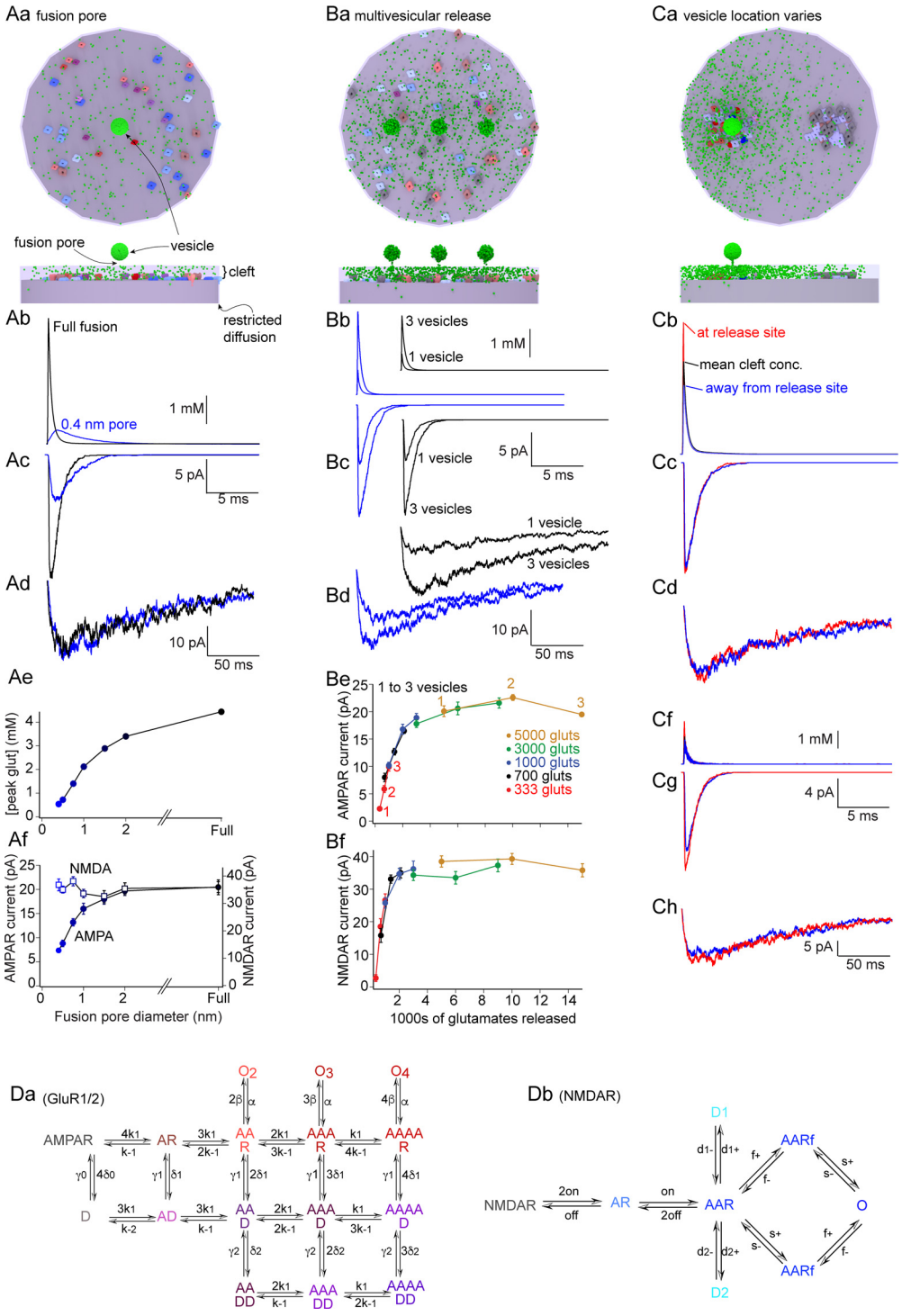

Figure 7. Simulating neurotransmitter release and receptor activation. ***Aa***, Simulated 300 nm diameter synapses, 20 nm deep synaptic clefts, and a 1.7 nm path at the edge to restrict fusion. Image is from 500 μs after the start of fusion. To simulate a fusion pore, fusion started from a pore at fixed diameter (0.4 nm for 20 ms) before fully opening (***Aa***) or pores that fully opened within 200 μs. Simulated receptors were randomly seeded on the postsynaptic surface (receptor colors as for kinetic models, ***D***). ***Ab***, Varying initial fixed pore diameters slowed glutamate release, reduced its cleft concentration (graphed in ***Ae***), and differentially inhibited AMPA (***Ac***) over NMDA (***Ad***) receptor-mediated responses (graphed in ***Af***; filled circles represent AMPA; hollow squares represent NMDA). ***Ba***, Simulated MVR pattern. Three simulated vesicles where vesicle number was varied from 3 to 1 with 333-5000 glutamates/vesicle. ***Bb***, The effect on cleft glutamate concentration of reducing vesicle numbers from 3 to 1 when each contained either 1000 glutamates (blue) or 700 glutamates (black). The AMPAR response (***Bc***) and the NMDAR responses (***Bd***) are shown below. Graphs represent the AMPAR (***Be***) and the NMDAR responses (***Bf***). To each condition, both varying glutamates/vesicle (color-coded) and number of vesicles each point in the colored sections. ***Ca***, The effect of varying the position of the release site with respect to postsynaptic clustered receptors was simulated. Two receptor clusters were seeded with a mean separation of 150 nm and the releasing vesicle positioned over one. ***Cb***, Cleft glutamate concentrations over the clusters (red at release site, blue away from release) and mean cleft concentration (black) after 5000 glutamates were released in 200 μs. ***Cc***, AMPAR responses simulated under the release site (red) and away from the site (blue). ***Cd***, NMDAR responses. ***Cf-Ch***, Similar experiment to ***Cb-Cd***, but with 1500 glutamate molecules to reveal modulation of AMPAR- and NMDAR-mediated responses. ***Da***, Kinetic model for AMPARs and (***Db***) for NMDARs (parameters in Table 1). Colors are the same as shown for receptors in ***Aa***, ***Ba***, and ***Ca***.

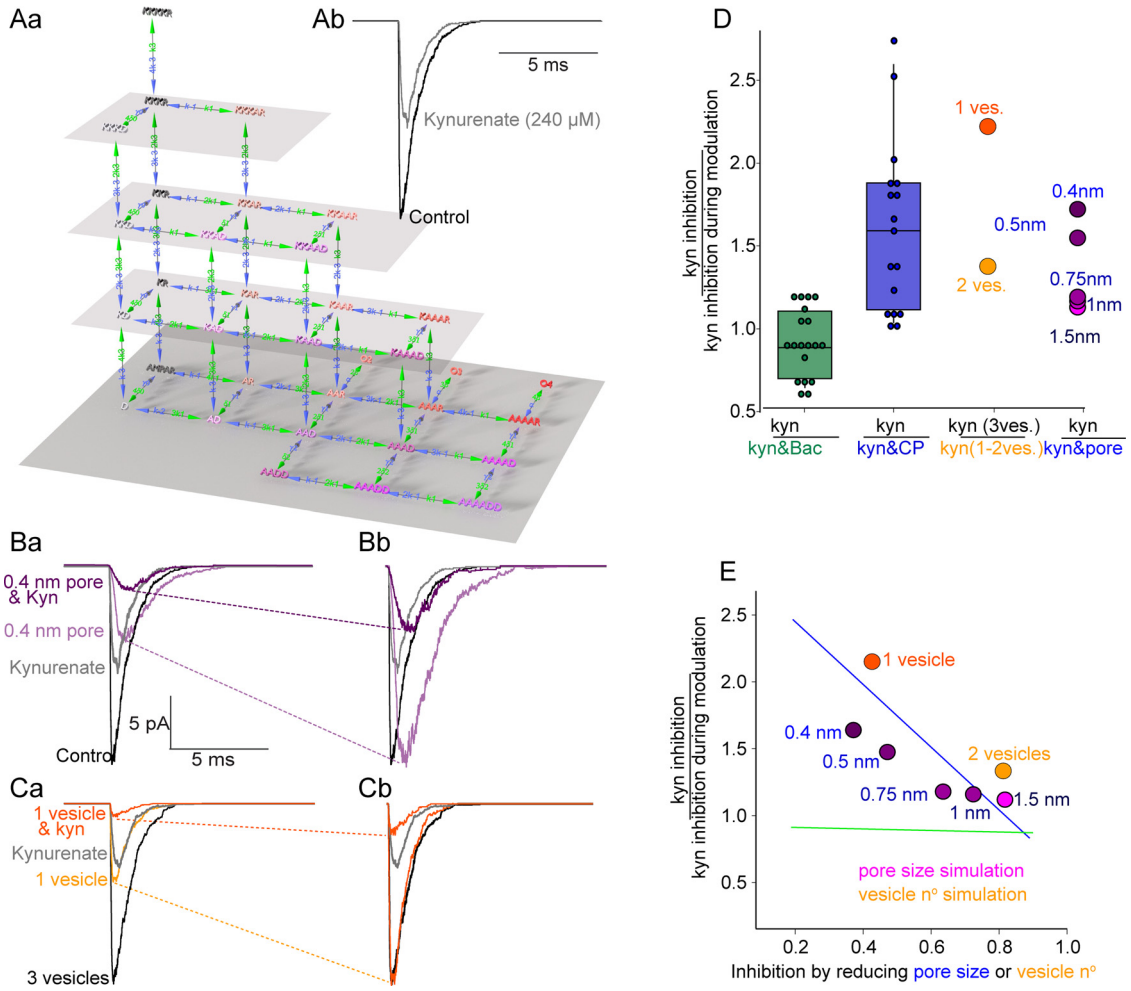

Figure 8. Simulating cleft glutamate modulation and kynurenate inhibition. ***Aa***, Kinetic model of AMPAR activation by glutamate and block by kynurenate. Colors and lowest tier of 3D model are as for Figure 7*Da*. Vertical elements of the 3D representation show kynurenate occupying receptor bound and desensitized states (parameters in Table 1). ***Ab***, Simulated full fusion in 200 μs with 5000 glutamates (black, control) and the effect of 240 μM kynurenate (gray). ***Ba***, The effect of kynurenate (gray) on control simulated responses (black) and on the response when the vesicle fusion pore was restricted to 0.4 nm (light purple without, purple with kynurenate). ***Bb***, Full fusion responses and 0.4 nm pore responses scaled to emphasize effect of kynurenate is amplified by the 0.4 nm pore. ***Ca***, Simulation as numbers of vesicle were varied from 3 to 1, each with 700 glutamates as in Fig. 7*Bb-Bd*. Effect of kynurenate (gray) on 3 vesicle response (black), and on 1 vesicle response (light orange) plus kynurenate (orange). ***Cb***, Responses scaled to compare effect of kynurenate on the 3 vesicle and 1 vesicle responses. ***D***, Comparison of magnification of kynurenate inhibition by baclofen (green) and CP93129 (blue) from experimental data (Fig. 3*E*) to the effect on kynurenate inhibition in simulations of reducing vesicle numbers (orange) or changing the initial fixed vesicle pore diameter (purple). ***E***, Simulation data (from ***D***) plotted against the effect of reducing vesicle number (orange) or fusion pore size (purple) on AMPAR responses. Green line indicates the fit to the similar effect of kynurenate on variations in experimental baclofen inhibition (from Fig. 3*G*). Blue line similarly indicates experimental CP93129 variation (from Fig. 3*H*).

antagonist, and its simulation, the experimental data can be explained by a reduction synaptic cleft glutamate. Results with kynurenate alone, however, do not discriminate between the effect on release, whether change in fusion pore diameter or change in fusing vesicle numbers that causes this change in concentration.

Modulation of the time course of the AMPAR-mediated response

Simulating the slowing of the fusion pore opening slowed the rise and decay times of the simulated AMPAR response (Fig. 7*Ac*) demonstrated by replotting the inhibited response scaled to the peak of the control (Fig. 9*A*). In simulated data, the arrested pore diameter (0.4 nm) increased the time course (τ) of the rise from 0.09 to 0.35 ms and of the decay from 0.97 to 1.59 ms measured by single exponentials fitted to the rise and decay. Simulated kinetic properties of AMPAR opening are more rapid than those experimentally obtained. This may be because they are neither affected by dendritic filtering nor by asynchronous vesicle fusion. Nevertheless, we investigated effects of agonist on the kinetics of synaptic responses.

Responses from 11 neurons were recorded in which EPSCs showed monotonic decays (Fig. 9*B*). CP93129 (50 nM) increased τ's of rise and decay phases, visible when the response in CP93129 was scaled to the control amplitude (Fig. 9*Bb*). Single exponential fits to the 10%-90% rise times showed a significant increase from a mean of 1.4 to 2.0 ms ($t_{(10)}$ = 3.06, p = 0.006) as did the decay times from 7.3 to 9.4 ms ($t_{(10)}$ = 3.54, p = 0.003) (Fig. 9*B*).

Simulations of reduction of P_r between synapses is trivial, a reduction in numbers of sites; consequently, kinetic properties of the simulated EPSC are unchanged (Fig. 9*C*, left). Alternatively, a simulated reduction in P_r at a multivesicular synapse shows a slight decrease in decay rate (Fig. 9*C*, right). We compared this to effects of baclofen (1 μM), which reduces P_r, in 10 neurons, again in which the decay was monotonic. Baclofen had no

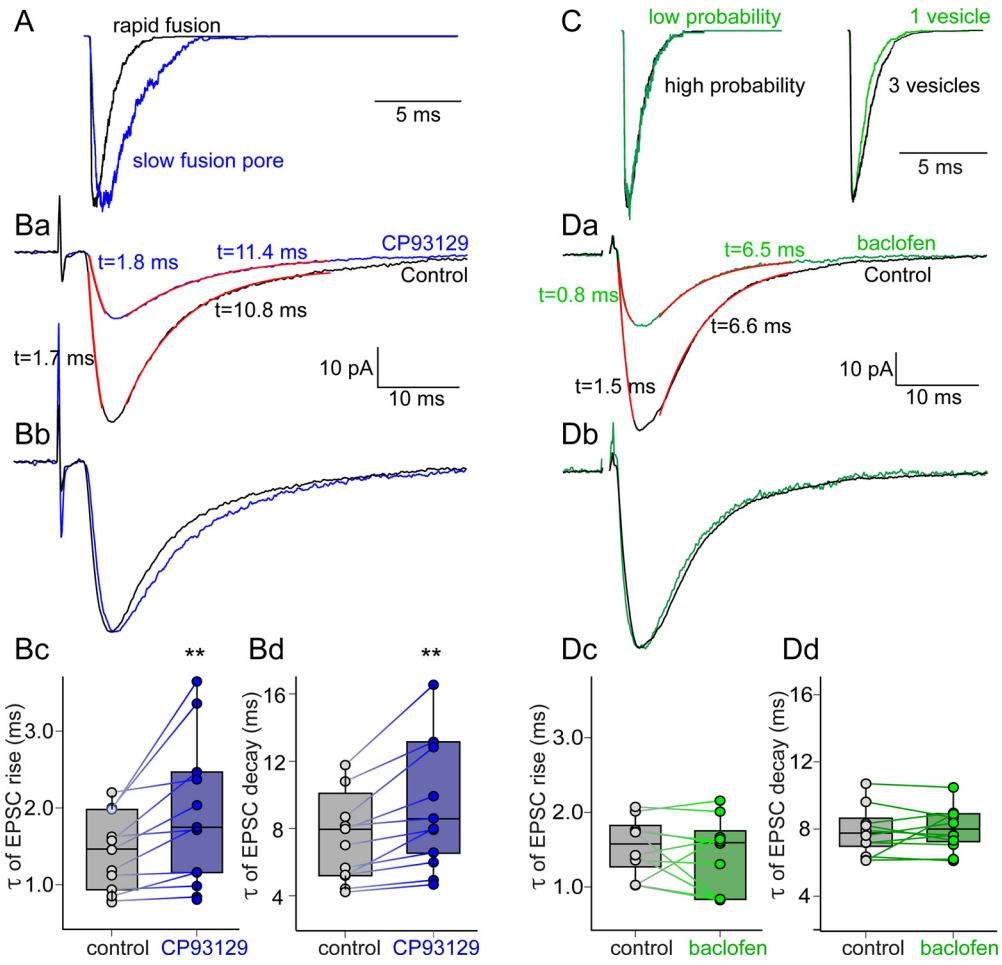

Figure 9. Effect of agonist on AMPA-mediated EPSC kinetics. ***A***, Data from simulating full fusion and a 0.4 nm pore scaled to the same amplitude to show the slowing of the rise and decay times of the resultant AMPAR-mediated response. ***Ba***, Experimental data of control responses (mean of 10 sequential EPSCs, black) and responses in the same neuron in CP93129 (50 nM, blue). Red curves are single exponentials fitted to 10%-90% of the rise and of the decay phases. ***Bb***, Response amplitudes scaled to emphasize the change in rates of the response in CP93129. ***Bc***, Box plots and data points for the rise time in control (gray) and in CP93129 (blue). ***Bd***, For decay times. ***C***, Simulated AMPA-mediated EPSCs scaled to show the kinetic effect of reduced number of responses to mimic a change of P_r at univesicular synapses on simulated kinetics (right) or reduced number of vesicles (from 3 to 1) at multivesicular synapses (left). ***Da***, Experimental control responses (black) and in the same neuron in baclofen (600 nM, green). Red curves indicate single exponentials fitted to rise and decay phases as in ***B***. ***Db***, Response amplitudes scaled as in ***B***. ***Dc***, Box plots and data points for the rise time in control (gray) and in baclofen (green). ***Dd***, Similarly for decay times. $^{**}p < 0.01$.

significant effect on mean rise time (control = 1.56 ± 0.12 ms, baclofen = 1.44 ± 0.16 ms; $t_{(9)}$ = 0.83, p = 0.21) or decay (control = 7.92 ± 0.47 ms, baclofen = 8.11 ± 0.41 ms; $t_{(9)}$ = 0.59, p = 0.30) (Fig. 9*D*). These results emphasize that 5-HT_{1B} and $GABA_B$ receptors on the same presynaptic terminals mediate inhibition by different mechanisms.

Repetitive stimulation and train-dependent responses

At the same terminals, $GABA_B$ receptors inhibit Ca^{2+} entry, whereas 5-HT_{1B} receptors cause G$\beta\gamma$ to interfere with Ca^{2+}-synaptotagmin SNARE complex interactions (Hamid et al., 2014). This implies selective effects of receptor activation, but also synergy following activation of both receptors (Zurawski et al., 2019). As presynaptic Ca^{2+} accumulates during stimulus trains (Yoon et al., 2007; Hamid et al., 2014) that induce long-term plasticity (O'Keefe, 1990), it may modify competition for interaction with the SNARE complex between G$\beta\gamma$ and synaptotagmin or other Ca^{2+} sensors, such as Doc2 (Groffen et al., 2006) or synaptotagmin 7 (Jackman et al., 2016; Jackman and Regehr, 2017).

$GABA_B$ receptors inhibit train-dependent Ca^{2+} accumulation. To show this, we recorded Ca^{2+} transients in CA1 pyramidal neuron terminals by filling the axons with Ca^{2+}-sensitive dyes. CA1 neurons were whole-cell recorded under current clamp with a red dye (Alexa-594) to determine the axon location and a Ca^{2+}-sensitive dye (Fluo 5F) to record action potential evoked Ca^{2+} transients. We have previously shown that Fluo 5F allows reliable recording of Ca^{2+} signals (Hamid et al., 2014, 2019). Individual presynaptic varicosities in the subiculum were imaged using line scanning (500 Hz) and neurons stimulated with 2 ms depolarizing current pulse trains (5 stimuli at 20 ms intervals) to evoke action potentials (Fig. 10*A*, top). Line scanning resolved Ca^{2+} transients over accumulating Ca^{2+} during the stimulus train (Fig. 10*Aa*, bottom). Baclofen (600 nM) reduced the Ca^{2+} transient following each stimulus in the train (Fig. 10*Ac*, green squares). The last transient was reduced to 0.46 ± 0.07 of control ($t_{(3)}$ = 2.94, p = 0.049). CP93129 (100 nM) had no effect on the train-evoked Ca^{2+} transients (Fig. 10*Ac*, blue circles). The last transient in the train in CP9319 was 1.18 ± 0.11 of control ($t_{(3)}$ = 1.55, p = 0.13). The absolute value of Ca^{2+} surrounding synapses may be lower than used in these recordings (Borst, 2010), although the values of P_r that we obtained from iGluSnFr experiments were similar, but the overall finding that 5-HT_{1B} receptor effects are both Ca^{2+} and train dependent holds true.

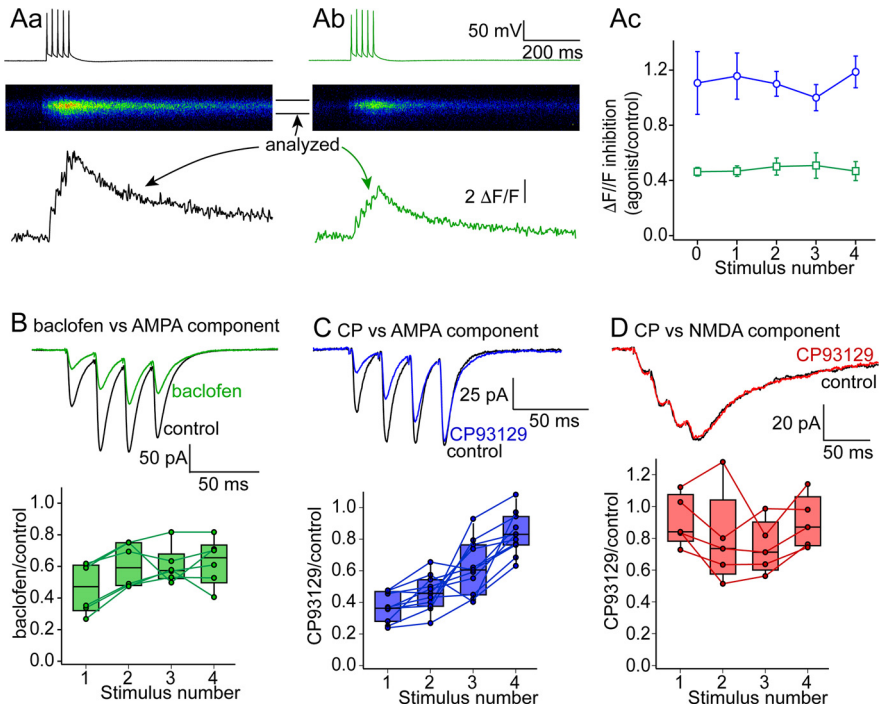

Figure 10. Effect of repetitive stimulation on inhibition. ***A***, Line scans through single CA1 neuron presynaptic varicosities imaged from neurons filled with Ca^{2+} dye (Fluo5F) from whole-cell patch recordings. ***Aa***, A train of 5 action potentials (top) were triggered via the patch pipette to evoke a train of fluorescence transients in the varicosity (middle) that were quantified (bottom). ***Ab***, Baclofen (600 nM) did not prevent evoked events but reduced the Ca^{2+} transient amplitude following each action potential. ***Ac***, Means of peak amplitudes in baclofen divided by pre-agonist control (green squares) of the peak of each transient in the train, from 4 varicosities. In contrast, in a further 4 varicosities, CP93129 (1 μM, blue circles) had no effect on transient amplitudes throughout trains. ***B***, Train of stimuli (4 shocks, 50 Hz) applied to CA1 axons to evoke AMPA EPSCs recorded in subicular neurons (in D-AP5 and bicuculline at a holding potential of −60 mV). Baclofen (1 μM) inhibited EPSCs throughout the train of stimuli. ***C***, A similar train stimulus applied for isolated AMPAR-mediated EPSCs in which box plots and raw data are as for ***B***. CP93129 (400 nM, blue) inhibited the first response in the train, but the EPSCs recovered to control amplitudes by the fourth stimulus. ***D***, A similar train stimulus applied in a preparation superfused with NBQX and bicuculline to isolate the NMDAR EPSCs. EPSCs were recorded at −35 mV to eliminate Mg^{2+} block of the NMDAR. CP93129 (400 nM) had little effect on any of the responses in the stimulus train. Box plots and raw data as for ***B***.

Consequently, we hypothesized that modifying Ca^{2+} entry with $GABA_B$ receptors will alter the efficacy of 5-HT_{1B} receptors during repetitive activity to provide a form of meta-modulation and synaptic integration. To address this, we first examined effects of stimulus trains (4 shocks, 50 Hz) on inhibition of synaptic responses by CP93129 and baclofen. AMPA EPSCs were isolated in bicuculline and D-AP5. Baclofen inhibited AMPA EPSCs (measured from EPSC initial slopes) throughout these trains with no significant difference in inhibition between responses within the train other than the paired-pulse enhancement (see Fig. 2) (Fig. 10*B*, ANOVA single factor $F_{(3,20)} = 28.2$, $p = 0.18$). In CP93129 (100 nM), initial slopes of the first responses were reduced to 42 ± 3% of control, while the fourth only to 78 ± 9% (Fig. 10*C*, single factor ANOVA determined whether CP93129 differentially altered EPSCs in the train; this was significant, ANOVA single factor $F_{(3,40)} = 28.2$, $p = 5.7 \times 10^{-10}$). *Post hoc* Tukey HSD analysis demonstrated the third and fourth EPSCs were inhibited significantly less than the first ($p < 0.001$). No significant inhibition of NMDA EPSCs isolated in bicuculine (5 μM) and NBQX (5 μM) was recorded for any stimulus (Fig. 10*D*, ANOVA single factor $F_{(3,16)} = 0.36$, $p = 0.78$).

GPCRs filter the final output of the hippocampus

$GABA_B$ receptors provide fairly uniform inhibition of synaptic output during stimulus trains after the second stimulus (Fig. 10*B*), when paired-pulse facilitation associated with changes in P_r is increased. By contrast, 5-HT_{1B} receptor activation reveals a complex modification of synaptic outputs from the hippocampus. NMDAR-mediated EPSCs are barely affected, although *in vivo* activation of the NMDA responses would require depolarization, which can be provided by synaptic transmission via AMPARs. AMPAR responses are blocked at the start but not the end of short stimulus trains. If 5-HT_{1B} receptor activation merely inhibited AMPAR responses, then synaptically evoked depolarization would be blocked and NMDARs would remain blocked by Mg^{2+}. Therefore, we first determined how 5-HT_{1B} receptors modify information flow between CA1 and subicular neurons during activity trains in which AMPAR-mediated depolarization triggers NMDAR-mediated responses (Herron et al., 1986).

We stimulated CA1 axons with short stimulus trains as earlier but recorded from subicular neurons under current-clamp conditions. Stimulation intensity was adjusted (up to 20 μA) to ensure that the first stimulus of the burst invariably caused an action potential in the recorded postsynaptic cell (Fig. 11*Aa*). We found a complex mode of inhibition, mediated by CP93129. After application of the agonist, the first EPSP is significantly inhibited, leading to a dose-dependent delay in depolarization and consequent firing of an action potential (Fig. 11*A–D*), but CP93129 did not prevent action potential firing during the train, even at saturating concentrations. The mean number of action potentials following the first stimulus in 4 cells was 1.3 ± 0.2 in control, but reduced to 0.2 ± 0.1 by a half-maximal concentration of CP93129 (50 nM, $p < 0.05$, Fig. 11*Ea*). However, firing recovered by the second stimulus, in which the control stimulus evoked 1.1 ± 0.4 action potentials and stimuli in CP93129, evoked 1.1 ± 0.4 (Fig. 11*Eb*), while by the third stimulus, evoked action potentials were enhanced by CP93129 (from 0.4 ± 0.2 to 0.7 ± 0.3, increase in number from first to third was significant, $p < 0.01$). Thus, while we see a concentration-dependent CP93129-evoked delay of action potentials (Fig. 11*A-D*). The mean area under the depolarization is barely altered (86 ± 5% of control at 1 μM), even when the first AMPAR-mediated response is substantially inhibited (to 10 ± 2%, Fig. 11*F*). This reflects the frequency-dependent recovery from 5-HT_{1B} receptor-mediated inhibition and lack of a CP93129 effect on NMDAR-mediated EPSCs.

Baclofen inhibits EPSCs throughout trains (Fig. 10*B*), and has previously been shown to act by inhibiting Ca^{2+} entry (Hamid et al., 2014). This implies that it can modify Ca^{2+}-synaptotagmin competition with G$\beta\gamma$ at SNARE complexes and consequently meta-modulate effects in CP93129 which causes G$\beta\gamma$ competition with Ca-synaptotagmin at SNARE complexes (Yoon et al., 2007). We investigated combined receptor activation on

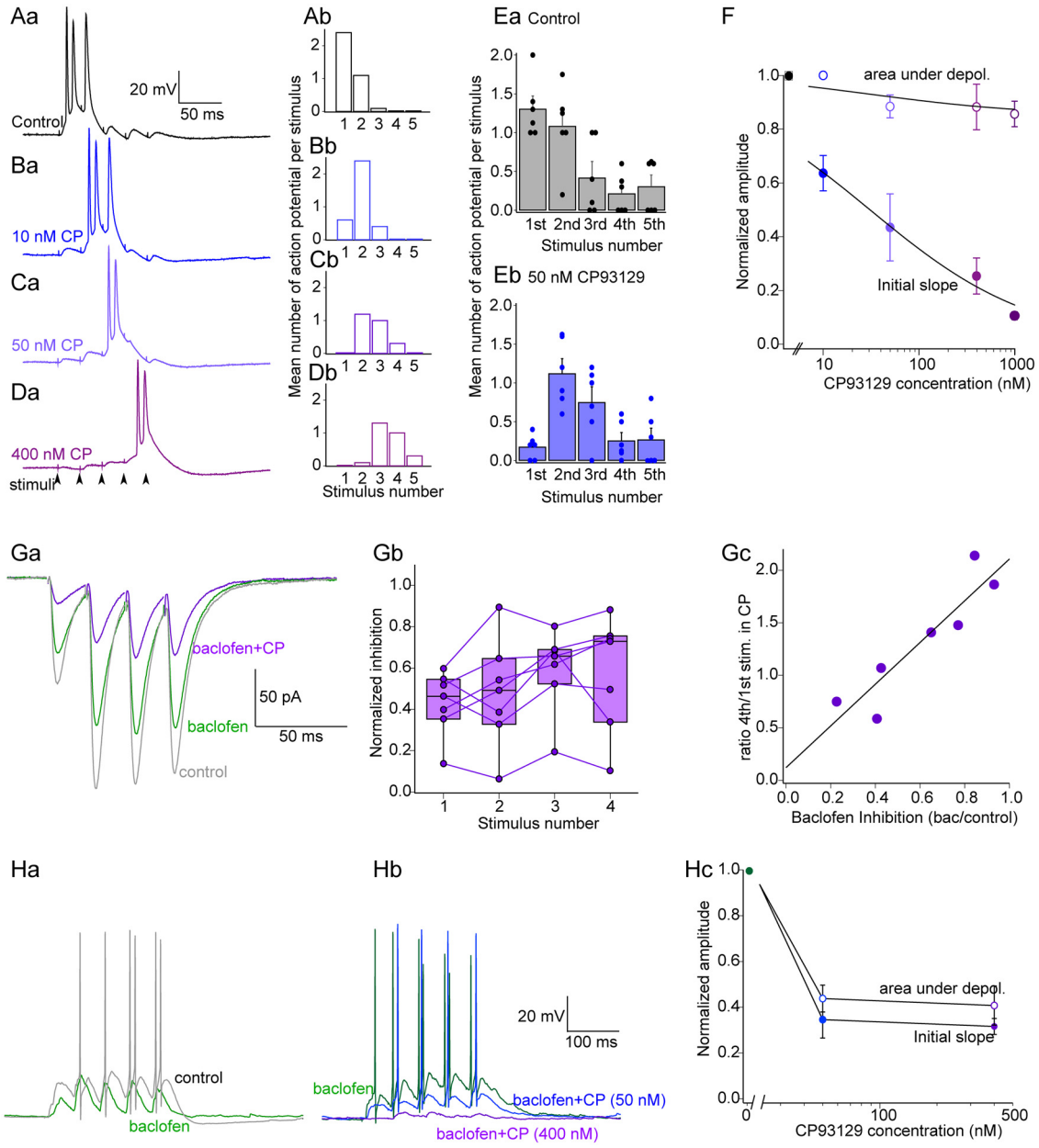

Figure 11. 5-HT_{1B} receptors filter synaptic output of the hippocampus, but these filter properties are modified by $GABA_B$ receptors. ***A***, 5-HT_{1B} receptors suppress activity at the start of a train but not total activity. A stimulus train (5 shocks, 50 Hz) was applied to CA1 axons, EPSPs recorded from subicular neurons. Stimulus intensity was adjusted to ensure the first train stimulus caused an action potential. ***Aa***, Example control trace. ***Ab***, Histogram shows mean number of action potentials following each stimulus from 10 sequential trains from this cell. ***Ba-Da***, Recordings of the cell in ***A*** after increasing concentrations of CP3129 (CP). ***Bb-Db***, Action potential counts from each stimulus in the recordings. ***E***, Mean action potential counts from each stimulus from 4 cells (***Ea***) in control and (***Eb***) in 50 nM CP93129. ***F***, CP93129 inhibits the first EPSP but not total excitation during trains. From 4 cells, a comparison of dose dependence of CP93129 inhibition of the mean EPSP initial slope on stimulus 1 and mean area under the depolarization for all stimuli (data normalized to control). ***G***, $GABA_B$ receptor activation modifies the filtering effect of 5-HT_{1B} receptors. ***Ga***, As shown in Figure 10, baclofen (green) 1 μM inhibits EPSPs uniformly throughout the stimulus train. CP93129 (400 nM purple) in the presence of baclofen now also inhibits uniformly throughout the train. Examples are mean responses from 10 sequential trains in one cell. ***Gb***, Box plots and single data show effects in 7 neurons of adding CP93129 (400 nM) to baclofen on responses from each of the 4 stimuli in the train. ***Gc***, The effect of CP93129 on the last EPSC in the train is proportional to the initial inhibitory effect of baclofen. ***Ha***, The modulating effect of baclofen 1 μM on CP93129 inhibition is seen in current-clamp recordings. Baclofen (green) inhibited EPSPs throughout the train. ***Hb***, In the same recording in baclofen, the stimulation intensity was increased (green). CP93129 was added at 50 nM (light blue) and 400 nM (dark blue). EPSPs in baclofen were now uniformly inhibited throughout the stimulus train. ***Hc***, Graph of amplitudes normalized to response in 1 μM baclofen for the first EPSP in the train and for the total area under the depolarization in increasing CP3129 concentrations.

presynaptic modulation. Baclofen (1 μM) inhibited AMPAR EPSCs uniformly during stimulus trains (Fig. 11*Ga*, green). However, in baclofen, CP93129 now also inhibits EPSCs throughout the train (Fig. 11*Ga*,*Gb*, purple). This meta-modulation of CP93129 inhibition by baclofen depends on the initial efficacy of baclofen. Plotting initial effects of baclofen alone against CP93129 inhibition of the last EPSC in the train in baclofen reveals a linear relationship (Fig. 11*Gc*). This is consistent with $GABA_B$ receptor inhibition of Ca^{2+} channels reducing Ca^{2+} that causes evoked release at each stimulus and for Ca^{2+}-synaptotagmin competition with 5-HT_{1B} receptor released G$\beta\gamma$ at SNARE complexes.

We tested this effect of baclofen on CP93129 filtering of EPSP trains. We did not evaluate specific effects of baclofen alone

because polysynaptic inhibition is also altered by baclofen, and these current-clamp experiments included no $GABA_A$ antagonists. Nevertheless, recordings in baclofen provided a starting condition to test effects of CP93129 during trains after partial inhibition of presynaptic Ca^{2+} entry by baclofen (Fig. 11*Ha*). CP93129 in baclofen reduced the area under the depolarization throughout the train (Fig. 11*Hb*), such that in contrast to the effects of CP93129 alone, in baclofen CP93129 equally inhibited the first EPSP slope and the area under the depolarization during the train. Changes in area and initial slope are not significantly different at 50 or 400 nM CP93129 (Fig. 11*H*; $t_{(7)} = 1.45$, $p = 0.19$ and $t_{(3)} = 1.39$, $p = 0.252$, respectively). Thus, different receptors with different effectors inhibit release with different temporal outcomes through train evoked responses, but they also interact such that one receptor ($GABA_B$) alters the effect of a second (5-HT_{1B}) both qualitatively and quantitatively causing an entirely novel form of presynaptic integration.

Discussion

Two well-characterized pathways mediate GPCR membrane-delimited presynaptic inhibition. G$\beta\gamma$ inhibits presynaptic Ca^{2+} entry or competes with Ca^{2+}-syt1 at the SNAP-25 c-terminal. $GABA_B$ receptors cause presynaptic inhibition throughout the CNS (Dutar and Nicoll, 1988; Alford and Grillner, 1991). They are thought to act principally via G$\beta\gamma$ inhibition of Ca^{2+} channels (Wu and Saggau, 1995; Hamid et al., 2014), although in the nucleus accumbens, they target SNARE complexes (Manz et al., 2019). Understanding their function is important given use of baclofen in disorders, such as multiple sclerosis, cerebral palsy, spinal injury, and stroke. Serotonin also modulates central excitability, and 5-HT1 receptors are found presynaptically. 5-HT_{1B} receptors control glutamate (Zifa and Fillion, 1992; Sari, 2004) and 5-HT (Davidson and Stamford, 1995) release, and play a role in delayed action of selective serotonin reuptake inhibitors (Svenningsson et al., 2006; Tiger et al., 2018), in anxiety and depression (Nautiyal et al., 2016). Two presynaptic targets have been found. In the calyx of Held, they reduce Ca^{2+} entry (Mizutani et al., 2006); and in lamprey, they modify synaptotagmin-SNARE interactions (Blackmer et al., 2001, 2005; Gerachshenko et al., 2005). $GABA_B$ and 5-HT_{1B} receptors colocalize at CA1 pyramidal neuron terminals (Boeijinga and Boddeke, 1993; Hamid et al., 2014) where 5-HT_{1B} receptors cause G$\beta\gamma$-SNAP-25 interactions, and $GABA_B$ receptors inhibit Ca^{2+} entry (Hamid et al., 2014; Zurawski et al., 2019). Why receptors colocalize to cause presynaptic inhibition via different mechanisms may depend on their intersecting signaling targets.

A third mechanism is possible, whereby neuromuscular miniature endplate potential frequency is reduced (Silinsky, 1984). Similarly, a mechanism independent of Ca^{2+} entry or interaction with c-terminal SNAP-25 inhibits mEPSCs in hippocampal neurons (Rost et al., 2011). The mechanisms that we have analyzed at CA1 terminals do not involve this effect. $GABA_B$ receptors inhibit Ca^{2+} entry, precluding effects on mEPSCs. G$\beta\gamma$ from 5-HT_{1B} receptors competes with syt1 to reduce release, but syt1 does not evoke mEPSCs (Pang et al., 2011; Vyleta and Smith, 2011); therefore, we would not expect G$\beta\gamma$ to alter mEPSCs. While G$\beta\gamma$-SNARE complex interaction might alter mEPSCs, clear results are hard to obtain because inputs to subicular pyramidal neurons come from mixed populations while only CA1 terminals express 5-HT_{1B} receptors. G$\beta\gamma$ might alter other Ca^{2+} sensor/SNARE interactions to mediate these effects (Yoon et al., 2008), but we have no evidence of this at CA1 synapses. Furthermore, we have previously demonstrated that 5-HT_{1B} receptors do not inhibit Sr^{2+}-evoked asynchronous release at CA1 terminals (Hamid et al., 2014). Sr^{2+} does not trigger fusion via syt1 SNARE interactions in reduced fusion models (Bhalla et al., 2005), indicating that asynchronous release is triggered by other fusogenic proteins (e.g., Doc2) (Yao et al., 2011).

Targets of presynaptic GPCRs determine their effects on neurotransmission. For example, Ca^{2+} channel inhibition reduces P_r; and in CA1 terminals, $GABA_B$ receptors enhance PPR, but leave synaptic glutamate concentration unaffected. They also equally inhibit NMDA and AMPA responses. In contrast, 5-HT_{1B} receptors do not change P_r. They leave PPRs unaffected, do not modify presynaptic Ca^{2+} entry (Hamid et al., 2014), but inhibit AMPA and NMDA EPSCs differentially. Therefore, we investigated variations in cleft glutamate.

Changing P_r with Mg^{2+} or baclofen left synaptic glutamate concentration unaltered, whereas 5-HT_{1B} receptors lowered it. We also found that 5-HT_{1B} receptors inhibited AMPAR-mediated EPSCs more than NMDA EPSCs. Low-affinity antagonism of NMDARs and AMPARs shows that cleft glutamate concentrations fall during 5-HT_{1B} receptor activation. Using iGluSnFr to visualize glutamate release revealed that 5-HT_{1B} receptors reduced the amount of glutamate released, but not the probability of each event. In contrast, $GABA_B$ receptor activation reduced the probability of recording an event on each stimulus. It increased the numbers of failures and reduced the number of discrete amplitudes recorded.

At least three explanations exist for these findings. (1) 5-HT reduces P_r where MVR predominates (Rudolph et al., 2015) and simultaneous fusion of multiple vesicles are linked (Singer et al., 2004). In this scenario, a change in P_r by 5-HT is hidden by delinking simultaneous fusion of multiple vesicles. (2) 5-HT modifies subsynaptic locations of release (Biederer et al., 2017; H. Chen et al., 2018). (3) A change in synaptic vesicle fusion mode.

We investigated these possibilities with experiments and simulations. We constructed Monte Carlo simulations of neurotransmitter release, diffusion, and activation of kinetic models of AMPARs and NMDARs. Simulations either changed numbers of vesicles fusing at active zones, altered the position of fusing vesicles with respect to postsynaptic receptors, or fusion pore timing. All these affected postsynaptic simulations of AMPAR activation. However, misalignment of fusion and receptors showed only small differential effects on AMPA and NMDA responses. MVR can govern cleft glutamate concentrations. This has been shown by investigating effects of repetitive stimulation on P_r (Foster et al., 2005; Christie and Jahr, 2006). Experimentally, we saw no change in glutamate cleft concentrations mediated by paired pulse stimulation to enhance P_r, or by reducing P_r with raised Mg^{2+} or baclofen. This implies that putative effects of 5-HT_{1B} receptors on MVR would be more complex than a change in P_r. In simulations we found that altering the number of vesicles fusing caused little differentiation between AMPARs and NMDARs. This contrasts with experimental effects of 5-HT_{1B}, but not $GABA_B$ receptors. Our simulations favored 5-HT_{1B} receptor-mediated effects on fusion pore dilation and duration and on P_r for $GABA_B$ receptors. Although the simulation does not account for all properties of biological fusion pores, such as charges lining a pore, or flickering (Chang et al., 2017), it is notable that sustaining a 0.4 nm pore best simulated experimental results. Biophysical data predict a similar fusion pore diameter before full fusion (Vardjan et al., 2013).

This conclusion is supported by experimental and simulated effects on response kinetics. Activation and decay rates following simulated arrested fusion pores were consistent with effects of 5-HT_{1B} receptors which similarly slowed EPSCs. In contrast, simulating changes in P_r, at multivesicular or between univesicular synapses, sped up the decay rate or left it unchanged, while baclofen had no effect on ESPC kinetics. By targeting the release machinery, 5-HT_{1B} receptors selectively change postsynaptic receptor activation. They are ineffective inhibitors of NMDA EPSCs. This is an effect previously ascribed to kiss-and-run fusion (Choi et al., 2003; Photowala et al., 2006; Schwartz et al., 2007; Gerachshenko et al., 2009).

High Ca^{2+} concentrations allow synaptotagmin to competitively prevent G$\beta\gamma$-SNARE complex binding, causing Ca^{2+}-dependent loss of G$\beta\gamma$-mediated presynaptic inhibition in lamprey (Yoon et al., 2007). Presynaptic Ca^{2+} accumulates during repetitive stimulation (Charlton et al., 1982; Swandulla et al., 1991). If 5-HT_{1B} receptors act by competing with Ca^{2+}-synaptotagmin SNARE interactions, whether syt1 or a fusogenic protein like synaptotagmin 7 (Jackman et al., 2016), we predict loss of 5-HT-mediated inhibition during repetitive stimulation. Indeed, we demonstrate that 5-HT_{1B} receptor-mediated inhibition is prevented at high Ca^{2+} concentrations and during repetitive stimuli. This suggests that 5-HT_{1B} receptors filter synaptic transmission with an outcome similar to a silent synapse (Liao et al., 1995). This prevents stray single action potential AMPA transmission. However, high-frequency stimuli, such as theta bursts, transmit efficiently.

In conclusion, the sensitivity of 5-HT_{1B} receptor effects to Ca^{2+} accumulation and their lack of effect on NMDA responses may underlie CP93129 actions on repetitive responses seen during current-clamp recordings of subicular neurons. 5-HT_{1B} receptors inhibit early responses in stimulus trains, but train stimulation allows recovery. Because NMDAR-mediated responses are much less inhibited, they may be recruited throughout burst evoked depolarizations, even after the first stimulation when NMDAR-mediated responses are blocked by Mg^{2+}, but the receptor is activated. Because NMDA responses are slow (Dale and Roberts, 1985; Lester et al., 1990), NMDARs are available for gating immediately following frequency-dependent release of inhibition of AMPA EPSPs and depolarization even during 5-HT_{1B} receptor activation.

We show that 5-HT_{1B} receptors change the profile of transmission of synaptic trains. They allow train stimuli to be transmitted but reject responses to single stimuli. Interestingly, 5-HT_{1B} KO mice display compromised working memory (Buhot et al., 2003), and reduced behavioral inhibition to novel stimuli, and learning is compromised in *SNAP-25Δ3* mice lacking G$\beta\gamma$ SNARE interactions (Zurawski et al., 2019). This receptor may play a role in behaviors requiring impulse control; for example, 5-HT_{1B} receptor KO animals are more motivated to self-administer cocaine (Rocha et al., 1998). Perhaps 5-HT_{1B} receptors selectively process information in the face of competing stimuli.

In contrast, $GABA_B$ receptors inhibit Ca^{2+} entry. This implies interaction between effects of $GABA_B$ and 5-HT_{1B} receptors because the effect of 5-HT_{1B} receptor activation is modified by Ca^{2+}-syt1. Indeed, low doses of baclofen modify temporal effects of CP93129 to prevent train-dependent recovery from CP9129's inhibition, showing that receptor coactivation integrates information. Even weak $GABA_B$ receptor activation prevents train-dependent recovery from 5-HT_{1B} receptor activation. Thus, colocalization of presynaptic receptors responding to different agonists but whose signaling pathways converge and interact allows presynaptic terminals to act as sites of neural integration. This complex interaction also points to the need to understand relationships between Ca^{2+}, release and modulation, and physiological Ca^{2+} concentrations may be lower than in this study.

References

Alabi AA, Tsien RW (2013) Perspectives on kiss-and-run: role in exocytosis, endocytosis, and neurotransmission. Annu Rev Physiol 75:393–422.

Alford S, Grillner S (1991) The involvement of $GABA_B$ receptors and coupled G-proteins in spinal GABAergic presynaptic inhibition. J Neurosci 11:3718–3726.

Asztely F, Erdemli G, Kullmann DM (1997) Extrasynaptic glutamate spillover in the hippocampus: dependence on temperature and the role of active glutamate uptake. Neuron 18:281–293.

Balaji J, Ryan TA (2007) Single-vesicle imaging reveals that synaptic vesicle exocytosis and endocytosis are coupled by a single stochastic mode. Proc Natl Acad Sci USA 104:20576–20581.

Banke TG, Traynelis SF (2003) Activation of NR1/NR2B NMDA receptors. Nat Neurosci 6:144–152.

Betke KM, Wells CA, Hamm HE (2012) GPCR mediated regulation of synaptic transmission. Prog Neurobiol 96:304–321.

Bhalla A, Tucker WC, Chapman ER (2005) Synaptotagmin isoforms couple distinct ranges of Ca^{2+}, Ba^{2+}, and Sr^{2+} concentration to SNARE-mediated membrane fusion. Mol Biol Cell 16:4755–4764.

Biederer T, Kaeser PS, Blanpied TA (2017) Transcellular nanoalignment of synaptic function. Neuron 96:680–696.

Blackmer T, Larsen EC, Takahashi M, Martin TF, Alford S, Hamm HE (2001) G protein betagamma subunit-mediated presynaptic inhibition: regulation of exocytotic fusion downstream of Ca^{2+} entry. Science 292:293–297.

Blackmer T, Larsen EC, Bartleson C, Kowalchyk JA, Yoon EJ, Preininger AM, Alford S, Hamm HE, Martin TF (2005) G protein betagamma directly regulates SNARE protein fusion machinery for secretory granule exocytosis. Nat Neurosci 8:421–425.

Boeijinga PH, Boddeke HW (1993) Serotonergic modulation of neurotransmission in the rat subicular cortex in vitro: a role for 5-HT_{1B} receptors. Naunyn Schmiedebergs Arch Pharmacol 348:553–557.

Boeijinga PH, Boddeke HW (1996) Activation of 5-HT_{1B} receptors suppresses low but not high frequency synaptic transmission in the rat subicular cortex in vitro. Brain Res 721:59–65.

Bonaventure P, Voorn P, Luyten WH, Jurzak M, Schotte A, Leysen JE (1998) Detailed mapping of serotonin 5-HT1B and 5-HT1D receptor messenger RNA and ligand binding sites in guinea-pig brain and trigeminal ganglion: clues for function. Neuroscience 82:469–484.

Borst JG (2010) The low synaptic release probability in vivo. Trends Neurosci 33:259–266.

Buhot MC, Wolff M, Benhassine N, Costet P, Hen R, Segu L (2003) Spatial learning in the 5-HT1B receptor knockout mouse: selective facilitation/impairment depending on the cognitive demand. Learn Mem 10:466–477.

Chang CW, Chiang CW, Jackson MB (2017) Fusion pores and their control of neurotransmitter and hormone release. J Gen Physiol 149:301–322.

Charlton MP, Smith SJ, Zucker RS (1982) Role of presynaptic calcium ions and channels in synaptic facilitation and depression at the squid giant synapse. J Physiol 323:173–193.

Chen BC, Legant WR, Wang K, Shao L, Milkie DE, Davidson MW, Janetopoulos C, Wu XS, Hammer JA, Liu Z, English BP, Mimori-Kiyosue Y, Romero DP, Ritter AT, Lippincott-Schwartz J, Fritz-Laylin L, Mullins RD, Mitchell DM, Bembenek JN, Reymann AC, et al. (2014) Lattice light-sheet microscopy: imaging molecules to embryos at high spatiotemporal resolution. Science 346:1257998.

Chen H, Tang AH, Blanpied TA (2018) Subsynaptic spatial organization as a regulator of synaptic strength and plasticity. Curr Opin Neurobiol 51:147–153.

Chen XK, Wang LC, Zhou Y, Cai Q, Prakriya M, Duan KL, Sheng ZH, Lingle C, Zhou Z (2005) Activation of GPCRs modulates quantal size in chromaffin cells through G(betagamma) and PKC. Nat Neurosci 8:1160–1168.

Choi S, Klingauf J, Tsien RW (2000) Postfusional regulation of cleft glutamate concentration during LTP at 'silent synapses.' Nat Neurosci 3:330–336.

Choi S, Klingauf J, Tsien RW (2003) Fusion pore modulation as a presynaptic mechanism contributing to expression of long-term potentiation. Philos Trans R Soc Lond B Biol Sci 358:695–705.

Christie JM, Jahr CE (2006) Multivesicular release at Schaffer collateral-CA1 hippocampal synapses. J Neurosci 26:210–216.

Clements JD, Lester RA, Tong G, Jahr CE, Westbrook GL (1992) The time course of glutamate in the synaptic cleft. Science 258:1498–1501.

Dale N, Roberts A (1985) Dual-component amino-acid-mediated synaptic potentials: excitatory drive for swimming in *Xenopus* embryos. J Physiol 363:35–59.

Davidson C, Stamford JA (1995) Evidence that 5-hydroxytryptamine release in rat dorsal raphe nucleus is controlled by 5-HT1A, 5-HT1B and 5-HT1D autoreceptors. Br J Pharmacol 114:1107–1109.

Del Castillo J, Katz B (1954) Quantal components of the end-plate potential. J Physiol 124:560–573.

Diamond JS, Jahr CE (1997) Transporters buffer synaptically released glutamate on a submillisecond time scale. J Neurosci 17:4672–4687.

Dobrunz LE, Stevens CF (1997) Heterogeneity of release probability, facilitation, and depletion at central synapses. Neuron 18:995–1008.

Dutar P, Nicoll RA (1988) Pre- and postsynaptic GABAB receptors in the hippocampus have different pharmacological properties. Neuron 1:585–591.

Elhamdani A, Azizi F, Artalejo CR (2006) Double patch clamp reveals that transient fusion (kiss-and-run) is a major mechanism of secretion in calf adrenal chromaffin cells: high calcium shifts the mechanism from kiss-and-run to complete fusion. J Neurosci 26:3030–3036.

Fang Q, Zhao Y, Herbst AD, Kim BN, Lindau M (2015) Positively charged amino acids at the SNAP-25 C terminus determine fusion rates, fusion pore properties, and energetics of tight SNARE complex zippering. J Neurosci 35:3230–3239.

Foster KA, Crowley JJ, Regehr WG (2005) The influence of multivesicular release and postsynaptic receptor saturation on transmission at granule cell to Purkinje cell synapses. J Neurosci 25:11655–11665.

Gandhi SP, Stevens CF (2003) Three modes of synaptic vesicular recycling revealed by single-vesicle imaging. Nature 423:607–613.

Gerachshenko T, Blackmer T, Yoon EJ, Bartleson C, Hamm HE, Alford S (2005) Gbetagamma acts at the C terminus of SNAP-25 to mediate presynaptic inhibition. Nat Neurosci 8:597–605.

Gerachshenko T, Schwartz E, Bleckert A, Photowala H, Seymour A, Alford S (2009) Presynaptic G protein-coupled receptors dynamically modify vesicle fusion, synaptic cleft glutamate concentrations and motor behavior. J Neurosci 29:10221–10233.

Groffen AJA, Friedrich R, Brian EC, Ashery U, Verhage M (2006) DOC2A and DOC2B are sensors for neuronal activity with unique calcium-dependent and kinetic properties. J Neurochem 97:818–833.

Haas KT, Compans B, Letellier M, Bartol TM, Grillo-Bosch D, Sejnowski TJ, Sainlos M, Choquet D, Thoumine O, Hosy E (2018) Pre-post synaptic alignment through neuroligin-1 tunes synaptic transmission efficiency. Elife 7:e31755.

Hamid E, Church E, Wells CA, Zurawski Z, Hamm HE, Alford S (2014) Modulation of neurotransmission by GPCRs is dependent upon the microarchitecture of the primed vesicle complex. J Neurosci 34:260–274.

Hamid E, Church E, Alford S (2019) Quantitation and simulation of single action potential-evoked Ca(2+) signals in CA1 pyramidal neuron presynaptic terminals. eNeuro 6:ENEURO.0343-19.2019.

Harata NC, Choi S, Pyle JL, Aravanis AM, Tsien RW (2006) Frequency-dependent kinetics and prevalence of kiss-and-run and reuse at hippocampal synapses studied with novel quenching methods. Neuron 49:243–256.

Herron CE, Lester RA, Coan EJ, Collingridge GL (1986) Frequency-dependent involvement of NMDA receptors in the hippocampus: a novel synaptic mechanism. Nature 322:265–268.

Hessler NA, Shirke AM, Malinow R (1993) The probability of transmitter release at a mammalian central synapse. Nature 366:569–572.

Hu Y, Qu L, Schikorski T (2008) Mean synaptic vesicle size varies among individual excitatory hippocampal synapses. Synapse 62:953–957.

Jackman SL, Regehr WG (2017) The mechanisms and functions of synaptic facilitation. Neuron 94:447–464.

Jackman SL, Turecek J, Belinsky JE, Regehr WG (2016) The calcium sensor synaptotagmin 7 is required for synaptic facilitation. Nature 529:88–91.

Kerr RA, Bartol TM, Kaminsky B, Dittrich M, Chang JC, Baden SB, Sejnowski TJ, Stiles JR (2008) Fast Monte Carlo simulation methods for biological reaction-diffusion systems in solution and on surfaces. SIAM J Sci Comput 30:3126.

Lein ES, Hawrylycz MJ, Ao N, Ayres M, Bensinger A, Bernard A, Boe AF, Boguski MS, Brockway KS, Byrnes EJ, Chen L, Chen L, Chen TM, Chin MC, Chong J, Crook BE, Czaplinska A, Dang CN, Datta S, Dee NR, et al. (2007) Genome-wide atlas of gene expression in the adult mouse brain. Nature 445:168–176.

Lester RA, Clements JD, Westbrook GL, Jahr CE (1990) Channel kinetics determine the time course of NMDA receptor-mediated synaptic currents. Nature 346:565–567.

Liao D, Hessler NA, Malinow R (1995) Activation of postsynaptically silent synapses during pairing-induced LTP in CA1 region of hippocampal slice. Nature 375:400–404.

Manz KM, Baxley AG, Zurawski Z, Hamm HE, Grueter BA (2019) Heterosynaptic GABAB receptor function within feedforward microcircuits gates glutamatergic transmission in the nucleus accumbens core. J Neurosci 39:9277–9293.

Marvin JS, Borghuis BG, Tian L, Cichon J, Harnett MT, Akerboom J, Gordus A, Renninger SL, Chen TW, Bargmann CI, Orger MB, Schreiter ER, Demb JB, Gan WB, Hires SA, Looger LL (2013) An optimized fluorescent probe for visualizing glutamate neurotransmission. Nat Methods 10:162–170.

Maschi D, Klyachko VA (2020) Spatiotemporal dynamics of multi-vesicular release is determined by heterogeneity of release sites within central synapses. Elife 9:e55210.

Mizutani H, Hori T, Takahashi T (2006) 5-HT1B receptor-mediated presynaptic inhibition at the calyx of Held of immature rats. Eur J Neurosci 24:1946–1954.

Nautiyal KM, Tritschler L, Ahmari SE, David DJ, Gardier AM, Hen R (2016) A lack of serotonin 1B autoreceptors results in decreased anxiety and depression-related behaviors. Neuropsychopharmacology 41:2941–2950.

Nimchinsky EA, Sabatini BL, Svoboda K (2002) Structure and function of dendritic spines. Annual Rev Physiol 64:313–353.

O'Keefe J (1990) A computational theory of the hippocampal cognitive map. Prog Brain Res 83:301–312.

Pang ZP, Bacaj T, Yang X, Zhou P, Xu W, Südhof TC (2011) Doc2 supports spontaneous synaptic transmission by a Ca(2+)-independent mechanism. Neuron 70:244–251.

Pawlu C, DiAntonio A, Heckmann M (2004) Postfusional control of quantal current shape. Neuron 42:607–618.

Photowala H, Blackmer T, Schwartz E, Hamm HE, Alford S (2006) G protein betagamma-subunits activated by serotonin mediate presynaptic inhibition by regulating vesicle fusion properties. Proc Natl Acad Sci USA 103:4281–4286.

Robert A, Howe JR (2003) How AMPA receptor desensitization depends on receptor occupancy. J Neurosci 23:847–858.

Rocha BA, Scearce-Levie K, Lucas JJ, Hiroi N, Castanon N, Crabbe JC, Nestler EJ, Hen R (1998) Increased vulnerability to cocaine in mice lacking the serotonin-1B receptor. Nature 393:175–178.

Rost BR, Nicholson P, Ahnert-Hilger G, Rummel A, Rosenmund C, Breustedt J, Schmitz D (2011) Activation of metabotropic GABA receptors increases the energy barrier for vesicle fusion. J Cell Sci 124:3066–3073.

Rudolph S, Tsai MC, von Gersdorff H, Wadiche JI (2015) The ubiquitous nature of multivesicular release. Trends Neurosci 38:428–438.

Rusakov DA, Kullman DM (1998) Extrasynaptic glutamate diffusion in the hippocampus: ultrastructural constraints, uptake, and receptor activation. J Neurosci 18:3158–3170.

Sari Y (2004) Serotonin1B receptors: from protein to physiological function and behavior. Neurosci Biobehav Rev 28:565–582.

Savtchenko LP, Rusakov DA (2007) The optimal height of the synaptic cleft. PNAS 104:1823–1828.

Schwartz EJ, Blackmer T, Gerachshenko T, Alford S (2007) Presynaptic G-protein-coupled receptors regulate synaptic cleft glutamate via transient vesicle fusion. J Neurosci 27:5857–5868.

Sigworth FJ (1983) Electronic design of the patch clamp. In: Single-channel recording (Sakmann B, Neher E, eds), pp 3–35. New York: Plenum.

Silinsky EM (1984) On the mechanism by which adenosine receptor activation inhibits the release of acetylcholine from motor nerve endings. J Physiol 346:243–256.

Singer JH, Lassova L, Vardi N, Diamond JS (2004) Coordinated multivesicular release at a mammalian ribbon synapse. Nat Neurosci 7:826–833.

Spruce AE, Breckenridge LJ, Lee AK, Almers W (1990) Properties of the fusion pore that forms during exocytosis of a mast cell secretory vesicle. Neuron 4:643–654.

Svenningsson P, Chergui K, Rachleff I, Flajolet M, Zhang X, El Yacoubi M, Vaugeois JM, Nomikos GG, Greengard P (2006) Alterations in 5-HT1B receptor function by p11 in depression-like states. Science 311:77–80.

Swandulla D, Hans M, Zipser K, Augustine GJ (1991) Role of residual calcium in synaptic depression and posttetanic potentiation: fast and slow calcium signaling in nerve terminals. Neuron 7:915–926.

Takahashi M, Freed R, Blackmer T, Alford S (2001) Calcium influx-independent depression of transmitter release by 5-HT at lamprey spinal cord synapses. J Physiol 532:323–336.

Tang AH, Chen H, Li TP, Metzbower SR, MacGillavry HD, Blanpied TA (2016) A trans-synaptic nanocolumn aligns neurotransmitter release to receptors. Nature 536:210–214.

Tedford HW, Zamponi GW (2006) Direct G protein modulation of Cav2 calcium channels. Pharmacol Rev 58:837–862.

Tiger M, Varnas K, Okubo Y, Lundberg J (2018) The 5-HT1B receptor: a potential target for antidepressant treatment. Psychopharmacology (Berl) 235:1317–1334.

Vardjan N, Jorgacevski J, Zorec R (2013) Fusion pores, SNAREs, and exocytosis. Neuroscientist 19:160–174.

Vardjan N, Stenovec M, Jorgacevski J, Kreft M, Zorec R (2007) Subnanometer fusion pores in spontaneous exocytosis of peptidergic vesicles. J Neurosci 27:4737–4746.

Vyleta NP, Smith SM (2011) Spontaneous glutamate release is independent of calcium influx and tonically activated by the calcium-sensing receptor. J Neurosci 31:4593–4606.

Wu LG, Saggau P (1995) GABAB receptor-mediated presynaptic inhibition in guinea-pig hippocampus is caused by reduction of presynaptic Ca^{2+} influx. J Physiol 485:649–657.

Yao J, Gaffaney JD, Kwon SE, Chapman ER (2011) Doc2 is a Ca^{2+} sensor required for asynchronous neurotransmitter release. Cell 147:666–677.

Yoon EJ, Gerachshenko T, Spiegelberg BD, Alford S, Hamm HE (2007) Gbetagamma interferes with Ca^{2+}-dependent binding of synaptotagmin to the soluble N-ethylmaleimide-sensitive factor attachment protein receptor (SNARE) complex. Mol Pharmacol 72:1210–1219.

Yoon EJ, Hamm HE, Currie KP (2008) G protein betagamma subunits modulate the number and nature of exocytotic fusion events in adrenal chromaffin cells independent of calcium entry. J Neurophysiol 100:2929–2939.

Zifa E, Fillion G (1992) 5-Hydroxytryptamine receptors. Pharmacol Rev 44:401–458.

Zurawski Z, Page B, Chicka MC, Brindley RL, Wells CA, Preininger AM, Hyde K, Gilbert JA, Cruz-Rodriguez O, Currie KP, Chapman ER, Alford S, Hamm HE (2017) G$\beta\gamma$ directly modulates vesicle fusion by competing with synaptotagmin for binding to neuronal SNARE proteins embedded in membranes. J Biol Chem 292:12165–12177.

Zurawski Z, Thompson Gray AD, Brady LJ, Page B, Church E, Harris NA, Dohn MR, Yim YY, Hyde K, Mortlock DP, Jones CK, Winder DG, Alford S, Hamm HE (2019) Disabling the G$\beta\gamma$-SNARE interaction disrupts GPCR-mediated presynaptic inhibition, leading to physiological and behavioral phenotypes. Sci Signal 12:scisignal.aat8595.